

© Copyright by Janakiram Kaushal Kadiyala 2018
All Rights Reserved

ATOMISTIC SIMULATIONS OF PARTICLE REINFORCED NANOCRYSTALLINE MATERIALS

A Thesis

Presented to

the Faculty of the Department of Mechanical Engineering

University of Houston

In Partial Fulfillment

of the Requirements for the Degree

Master of Science

in Mechanical Engineering

by

Janakiram Kaushal Kadiyala

December 2018

ATOMISTIC SIMULATIONS OF PARTICLE REINFORCED NANOCRYSTALLINE MATERIALS

Janakiram Kaushal Kadiyala

Approved:

Chair of the Committee
Yashashree Kulkarni, Associate Professor,
Mechanical Engineering

Committee Members:

Haleh Ardebili, Associate Professor,
Mechanical Engineering

Qianmei Feng, Associate Professor,
Industrial Engineering

Suresh K. Khator, Associate Dean,
Cullen College of Engineering

Pradeep Sharma, Professor and Chair,
Mechanical Engineering

ACKNOWLEDGEMENTS

It gives me immense pleasure to sincerely acknowledge the people who helped me in different ways to complete my thesis. I would like to express my deepest gratitude to my advisor, Dr. Yashashree Kulkarni, who has given me a wonderful opportunity to join her research team. It is a matter of pride, pleasure, and prestige that I could work under the esteemed guidance and supervision of my advisor. I would also like to extend my sincere gratitude to my committee members, Dr. Haleh Ardebili and Dr. Qianmei Feng for taking their valuable time out and giving me their insightful suggestions and recommendations. I also acknowledge Dr. Agarwal, Dr. Nakshatrala and Dr. Baxevanis for their excellent teaching in mechanics courses.

I am now pleased to gratify the resources provided by University of Houston to perform all my simulations. I especially thank Center for Advanced Computing and Data Science (CACDS) for providing access to the supercomputers and also for their friendly staff who offer expert consultation on using these systems.

I also acknowledge my professors in NIT Hamirpur, Dr. Rakesh Sehgal, Dr. Rajesh Sharma, Dr. Somesh Kumar and Dr. Anoop Kumar, who have made my practical concepts cleared in addition to their fine classroom teaching. I am indebted to have studied in the beautiful campus of NIT Hamirpur, which is probably the most beautiful college in India besides being one of the best colleges in the country academically.

I'm deeply indebted to my family for their relentless support and encouragement in the field of education. My father, Dr. KVSG Murali Krishna, who is a professor of JNTU-Kakinada, was my first teacher. He is the prime reason for my transformation to an above average student. It is always an honor to be the son of 'Best teacher award winner' for the state of Andhra Pradesh. I also acknowledge my grandfather, KVRK Sastry, who retired after teaching physics to me and my

brother after an incredible 60 years in the teaching field. He not only used to teach high school physics to me, but also used to discuss the lives of inspirational personalities, especially in the field of science. This elevated my interests in science, mainly physics. I also acknowledge my mom, Kameswari and brother, Kaushik who have been supportive all my life.

I am also thankful to my maternal uncles, Hanuma Kumar, a mechanical engineer in Shell and Naga Bhushan, a professor of Electronics. Both of them being in the field of engineering, were always concerned about my practical knowledge and always encouraged me to aspire to go for higher studies. I also appreciate my paternal aunt Lakshmi and my two cousins, Arvind and Prashant who did their master's in mechanical engineering in Germany for sharing their valuable suggestions in shaping my thesis. Last but not the least, I thank my Houstonian friends and my lab-mates for making my life away from home easier in these last few years.

ATOMISTIC SIMULATIONS OF PARTICLE REINFORCED NANOCRYSTALLINE MATERIALS

An Abstract
of a
Thesis
Presented to
the Faculty of the Department of Mechanical Engineering
University of Houston

In Partial Fulfillment
of the Requirements for the Degree
Master of Science
in Mechanical Engineering

by
Janakiram Kaushal Kadiyala
December 2018

ABSTRACT

Nanocrystalline materials have applications in numerous fields due to their high strength. Grain growth is prevalent in nanocrystalline materials and leads to a decrease in material strength. Zener pinning has proven to be effective in hindering grain growth and thus, maintain the strength of the material. In this work, atomistic simulations were performed to understand and visualize the effect of Zener pinning in restricting grain boundary motion, and hence grain growth. The simulations were performed on two different grain boundary structures, $\Sigma 5$ and $\Sigma 17$ by varying the particle diameter and distance between the particles and compare these results with that of structures without any particles. The impact of adding high particle volume fraction (up to 50%) in Ag polycrystals to produce ultrahigh strength materials is also discussed. The yield strength of these nanocomposites was evaluated by varying particle volume fraction, particle size and inter-particle spacing. The highest yield strength observed in Ag nanocomposites was found to be about 5 times the strength of nanocrystalline Ag. The possible strengthening mechanisms responsible for this huge increase are discussed based on molecular dynamics results.

TABLE OF CONTENTS

ACKNOWLEDGEMENTS	iv
ABSTRACT	viii
TABLE OF CONTENTS	ix
LIST OF FIGURES	xi
LIST OF TABLES	xiii
NOTATION	xiv
CHAPTER 1 INTRODUCTION	1
1.1 Background and Motivation	1
1.2 Scope of this work	3
1.3 Objectives of this work	3
1.4 Outline of the Thesis	3
CHAPTER 2 LITERATURE REVIEW	5
2.1 Nanocrystalline Materials	5
2.2 Grain Boundaries	8
2.3 Zener Pinning	10
2.4 Particle Reinforced Nanocomposites	12
CHAPTER 3 COMPUTATIONAL APPROACH	15
3.1 Molecular Dynamics	15
3.1.1 Interatomic Potential	16
3.1.2 Interaction Force	17
3.1.3 Energy Minimization	17
3.1.4 Equations of Motion	18
3.1.5 Visualization	18
3.1.6 Limitations	19

LIST OF FIGURES

Figure 2.1	TEM images of Nanocrystalline materials [1].	6
Figure 2.2	Comparison of stress-strain curves of nanocrystalline Cu and coarse grained Cu samples [2].	7
Figure 2.3	Stress-strain plots for Cu at different grain sizes [3].	7
Figure 2.4	Artistic representation of a grain boundary [4]. The colored atoms represent the different grains in material and the grey atoms (disordered) represent the grain boundary.	9
Figure 2.5	Effect of coherency of different types of particle on efficiency of pinning [5]. The pinning force depends on the constant K.	11
Figure 2.6	Effect of volume fraction of spherical particles on normalized yield strength in ductile metal matrix composites [6].	13
Figure 4.1	Σ 5 and Σ 17 grain boundaries generated using LAMMPS. The number of atoms in both the specimens were around 10,000.	24
Figure 4.2	Different regions defined in the GB specimens. The lower region was held fixed and shear was applied on the upper region.	25
Figure 4.3	Stress-strain and displacement-time curves of specimen X0 at 800 K with a shear velocity of 1 m/s.	26
Figure 4.4	Stress-strain and Displacement time curves of specimen Y0 at 800 K with a shear velocity of 1 m/s.	26
Figure 4.5	Stress-strain curve of specimen X1 at 800 K with a shear velocity of 1 m/s. Particle diameter = 4.4 Å.	27
Figure 4.6	Visualizations of Σ 5 tilt GB under shear strain. The pinning pressure provided by the particle counteracts the driving force of GB and this is a case of efficient pinning as GB motion is hindered.	27

Figure 4.7	Stress-strain curve of specimen Y1 at 800 K with a shear velocity of 1 m/s. Particle diameter = 4.4 Å.	28
Figure 4.8	Visualizations of Σ 17 tilt GB under shear strain. The driving force of GB is higher than the pinning force provided by the particle. Pinning is not as efficient as observed in Σ 5 tilt GB.	28
Figure 4.9	Stress-strain curve of specimen Y2 at 800 K with a shear velocity of 1 m/s. Particle diameter = 6.2 Å.	29
Figure 4.10	Stress-strain curve of specimen Y3 at 800 K with a shear velocity of 1 m/s. Particle diameter = 4.4 Å.	29
Figure 5.1	Visual of Specimen A0 as seen in OVITO. The number of atoms in the specimen was 827,774.	35
Figure 5.2	Deformation of specimen A3 under a compression strain. The strain rate used was $5 \times 10^8 \text{ s}^{-1}$	36
Figure 5.3	Snapshots of specimen A0 at different strains. The yield point was observed at a strain of about 3.69%.	38
Figure 5.4	Snapshots of specimen A3 at different strains. The yield point was observed at a strain of about 1.8%.	39
Figure 5.5	Effect of volume fraction on stress-strain curves of different specimens of type A.	39
Figure 5.6	Effect of volume fraction on normalized yield strength of different specimen types.	40
Figure 5.7	Effect of particle size and volume fraction on normalized yield strength of different specimens.	41
Figure 5.8	Effect of inter-particle spacing and volume fraction on normalized yield strength of different specimens.	42

LIST OF TABLES

Table 4.1	Different particle diameters used to study Zener pinning in sigma 17 grain boundary	23
Table 5.1	Description of different specimen types used in this study	35
Table 5.2	List of specimens of type A.	36
Table 5.3	List of specimens of type B.	37
Table 5.4	List of specimens of type C.	37

NOTATION

Abbreviations

bcc	body centered cubic
EAM	Embedded Atom Method
fcc	face centered cubic
hcp	hexagonal closed packing
LAMMPS	Large-scale Atomic/Molecular Massively Parallel Simulator
MD	Molecular Dynamics
MMC	Metal Matrix Composite
MMNC	Metal Matrix Nanocomposite
NC	Nano-Crystalline
OVITO	Open Visualization Tool

Symbols

σ/σ_0	normalized yield strength
σ	yield strength
#	number

Units

μm	micrometer
Å	angstrom
GPa	gigapascal
mm	micrometer
MPa	megapascal
nm	nanometer
ns	nanosecond

CHAPTER 1 INTRODUCTION

1.1 Background and Motivation

Nanomaterials are those materials that have at least one dimension in the nanometer range. Nanotechnology is a field that deals with the synthesis, characterization, exploration, and exploitation of nanostructured materials. Different types of nanomaterials include clusters, quantum dots, nanocrystals, nanowires, and nanotubes. These nanomaterials have vastly different properties when compared to the bulk materials. Nanotechnology advancements have shown vast increase in the last few decades as they have a wide range of applications in various industries such as aerospace, agriculture, automobiles, defense, electronics, energy, environment, medicine, and many.

Every material is made of atoms, and these atoms have a specific lattice structure (fcc, bcc, hcp, etc.) depending on the material. As naturally available materials do not have a perfect lattice structure, they are comprised of a large number of grains, which are groups of atoms of a perfect lattice structure. The typical grain size of naturally available materials is of the order of mm. Nanocrystalline (NC) materials are those materials that have a nanoscale grain size. NC materials have higher strength when compared to their coarse-grained counterparts. This strength relationship with grain size comes from the Hall Petch effect [7,8]. This relationship is discussed later in chapter 2.

The goal of material scientists is to study the structure and properties of materials such as metals, alloys, polymers, etc. and to obtain information to develop new materials with enhanced properties. Conducting experiments on nanomaterials is expensive, and hence, the use of atomistic simulations gained more attention over the past few years to study the structure, properties, and different deformation mechanisms of nanomaterials.

Nanocrystalline materials have high strength because of their lower grain size. Nanocrystalline materials, especially when the grain size is less than 100 nm, are known to have numerous defects present in the nanostructure. The deformation mechanisms in nanomaterials are significantly different from coarse-grained materials. Grain growth is one of the common phenomena in nanocrystalline materials at high temperature, and sometimes even at lower temperatures. This phenomenon is highly undesirable as grain growth leads to a decrease in the strength of the material and hence, needs to be hindered. Zener pinning is a common technique used to restrict grain growth [9]. The use of atomistic simulations to study and visualize the effect of Zener pinning in restricting grain growth is not done appreciably.

Zener pinning is the effect of adding particles to provide a pinning force that restricts the grain boundary motion. Zener pinning can increase the strength of NC materials by a small amount as the particles that pin the GB correspond to a lower volume fraction. NC materials already have a higher strength than coarse-grained materials. To create ultrahigh strength materials, nanocrystalline composites with high particle volume fraction can be used. There are continuum models that describe the properties of high-strength composites. The strength of metal matrix composites has an exponential relationship with the particle volume fraction [6, 10]. When a ductile matrix is used, the yield strength does not show a significant increase until it reaches a threshold value of about 30% [11]. An attempt is made in this work to know if this trend is valid in NC composites as well. As NC materials (metals) already have high strength (around 1 GPa), the NC composites are expected to have a yield strength of about 3 GPa or more and can be used in applications where ultrahigh strength is desired.

1.2 Scope of this work

Grain boundaries play an important role in the mechanical properties of nanocrystalline materials. In this thesis, the main focus is to perform atomistic simulations on grain boundary structures by adding particles and study the effect of pinning in restricting grain boundary motion in nanocrystalline materials. The impact of adding high volume fraction of particles in NC composites to produce ultrahigh strength structures is also assessed.

1.3 Objectives of this work

The objectives of this work are to use atomistic simulations to:

1. Study the effect of Zener pinning of low angle and high angle tilt grain boundaries by varying the particle size and inter-particle spacing.
2. Perform stress-strain analysis for $\Sigma 5$ and $\Sigma 17$ grain boundary structures with and without particles and compare the GB motion.
3. Study the effect of adding high volume fraction of particles on the yield strength of nanocrystalline composites with a ductile matrix.
4. Compare the results in (3) with existing continuum models to check their validity in nanocomposites.

1.4 Outline of the Thesis

The thesis is presented in 6 chapters. The background, motivation, scope, and objectives of this work were discussed in the previous sections of this chapter.

Chapter 2 reviews the literature on NC materials, grain boundaries and their importance, Zener pinning, polycrystals, metal matrix nanocomposites (MMNCs). Different experimental, theoretical, and modeling techniques involved to achieve high strength in NC materials are discussed.

Chapter 3 explains the computational approach in this work. As all the simulations were performed on LAMMPS, a molecular dynamics package, the basics of molecular dynamics are discussed. A brief overview is given on the components of molecular dynamics to give more idea on interatomic potential, interaction force, energy minimization, equations of motion, visualization, and limitations of MD.

Chapter 4 discusses the effect of Zener pinning on Σ 5 and Σ 17 tilt grain boundaries. The effect of particle size and inter-particle distance on grain boundary migration is studied using atomistic simulations, and these results are compared to the GB motion when no particles are present in the structures.

Chapter 5 discusses the effect of volume fraction and particle size on the yield strength of metal matrix NC composites. Various simulations on NC polycrystals with rigid particles are performed using LAMMPS to understand the deformation mechanisms responsible for the increase in the yield strength of these NC composites.

Chapter 6 presents the summary of the results in this work. The limitations of this work are discussed. The possible aspects of research that may be useful are proposed.

CHAPTER 2 LITERATURE REVIEW

Nanocrystalline (NC) materials have unique properties when compared to their coarse-grained counterparts. There are several mechanisms that explain this difference in the properties. The primary goal of any material scientist is to provide high strength structures with limited use of materials. Nanocrystalline materials have proven to have much higher strength than that of their bulk materials. Nanocrystalline materials are materials with a grain size of less than 100 nm. The interfaces between two grains are called grain boundaries and the field of grain boundaries a vital aspect to study to understand the intricate mechanisms involved in nanocrystalline materials. One way of increasing the strength of a material is by adding second phase particles. The following sections review the literature available on the different aspects related to nanocrystalline materials and the effect of adding second phase particles in the nanocrystalline materials.

2.1 Nanocrystalline Materials

Nanocrystalline materials were significantly researched from the late 1980s and early 1990s. There were hundreds of papers published in this field since then. Today, nanocrystalline materials have numerous applications in the areas of aerospace, automobiles, agriculture, electronics, energy, environment, and many [12–18].

In 1989, Gleiter [19] published a paper on nanocrystalline materials emphasizing the synthesis, structure, and properties of these unique materials. Regarding the mechanical properties of NC materials, the hardness is higher when compared to the coarse-grained materials. This is because of the excellent bonding of atoms in NC materials at lower temperatures, but their ability to densify easily at high tem-

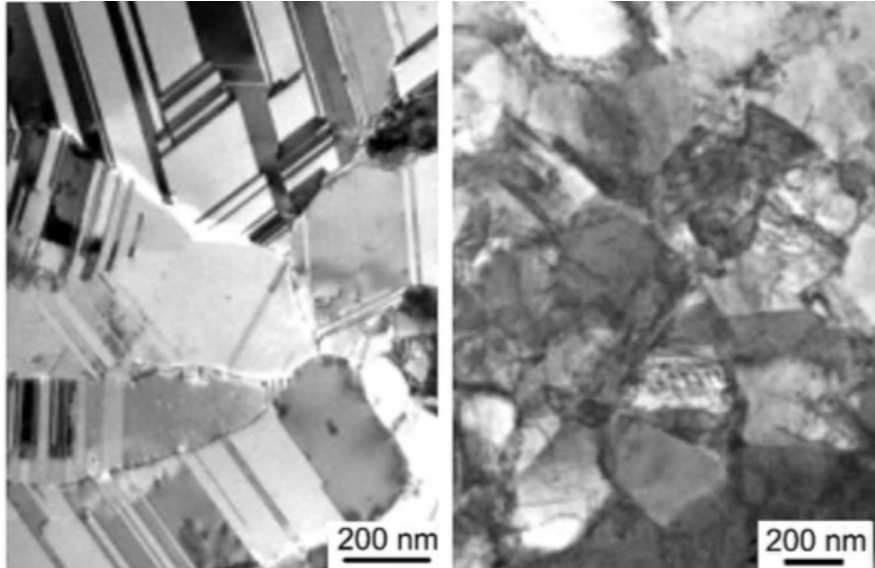


Figure 2.1: TEM images of Nanocrystalline materials [1].

peratures (above 700 K) due to increase in grain size can reduce their strength by a considerable amount.

Experiments on NC materials have shown that the yield strength of NC materials is significantly greater than that of their bulk counterparts. Figure 2.2 compares the strength of bulk NC Cu specimens prepared by in-situ consolidation ball milling method [2] and inert-gas condensation and compaction method [20] w.r.t. coarse-grained Cu sample with grain size greater than $80 \mu\text{m}$ as per the experimental investigation. As seen in the figure, the yield strength of NC materials is about 10 times higher than coarse-grained materials. This high strength of NC materials is an asset in applications where high strength is desired such as structural composites, heat sinks, EMI shielding, ballistic protection and aerospace components [21].

Hall-Petch relationship is widely known in the field of materials [22, 23]. The yield strength of a material is inversely proportional to the square-root of grain size. This expression is given as

$$\sigma = \mathbf{K} * \mathbf{d}^{-0.5}, \quad (2.1)$$

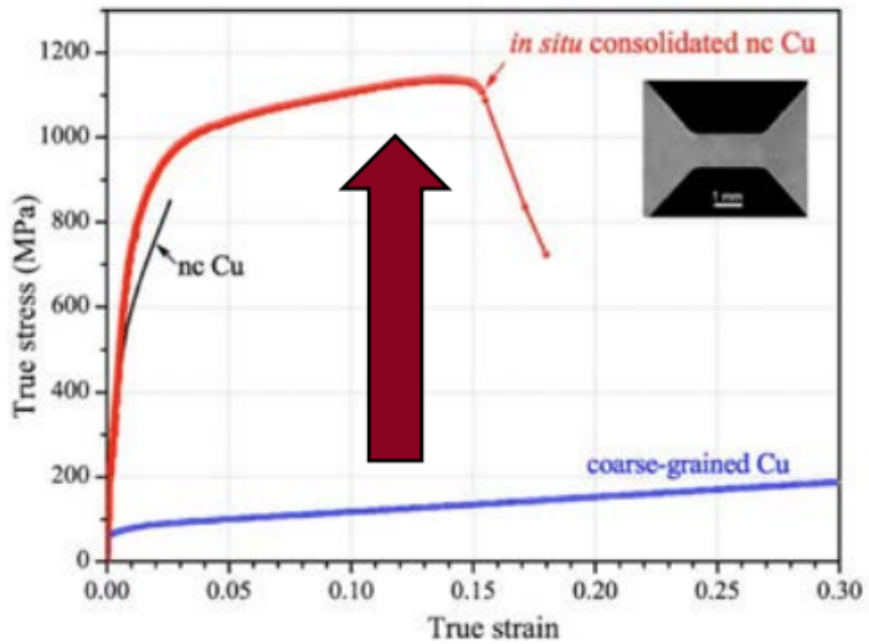


Figure 2.2: Comparison of stress-strain curves of nanocrystalline Cu and coarse grained Cu samples [2].

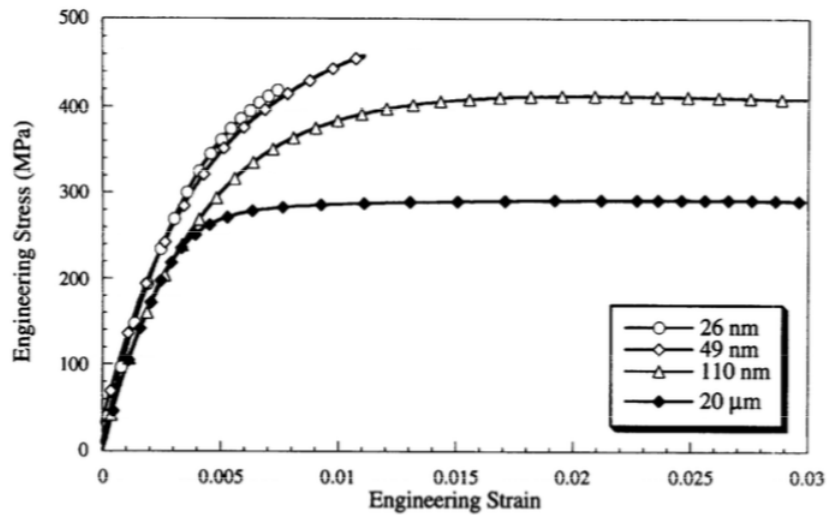


Figure 2.3: Stress-strain plots for Cu at different grain sizes [3].

where σ is yield strength of the material, d is the grain diameter, K is a constant that depends on the material. This phenomenon is also valid in NC materials [3,24] (figure 2.3). The strengthening of NC materials arises from the fact that the grain

boundaries block the dislocation motion and hence, making the plastic deformation more difficult at smaller grain sizes [25, 26].

In 2006, Van Swygenhoven, et al. [27] performed atomistic simulations on nanocrystalline fcc metals. They performed stress-strain analyses of different polycrystals whose average grain size was less than 100 nm. The results show that the yield strength of Cu polycrystals was related to the grain size approving Hall-Petch effect. The observed yield strength of these nanocrystalline specimens was about 1 GPa which is about 10 times that of coarse-grained Copper.

As the grain size reduces, the yield strength of a material increases. But this behavior is not observed when the grain size reaches below a threshold limit (about 10-30 nm) [28–31]. The yield strength of NC materials below this threshold grain size is known to reduce with a further decrease in grain size. This effect is observed in atomistic simulations [3, 32]. When the grain size reduces to a threshold limit, the dominating deformation mechanism changes from lattice dislocation activities to mechanisms such as grain boundary diffusional creep and softening behavior. This phenomenon is called as the inverse Hall-Petch effect. [24, 33, 34]

The presence of grain boundaries in the material determines the yield strength of the NC material. Hence, the study of grain boundaries is decisive in exploring NC materials. The next section on grain boundaries provides a brief overview on the grain boundary movement, grain growth, and other phenomena related to GBs in order to understand their effect on the strength of NC materials.

2.2 Grain Boundaries

Grain boundaries are the interfaces between two differently oriented grains as shown in figure 2.4. The grey-colored atoms in the figure represent the transition region corresponding to the GBs between different grains (represented in different

colors). The study of grain boundaries play a vital role in determining the strength of NC materials [35–37].

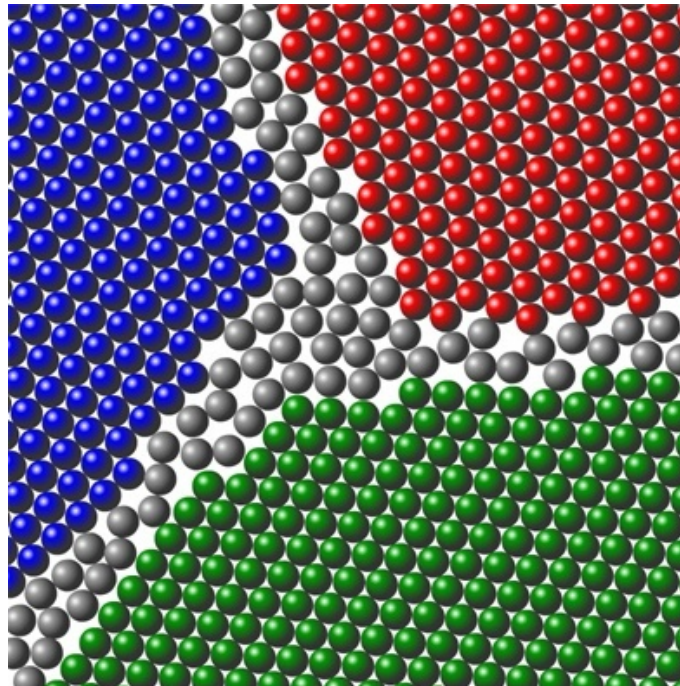


Figure 2.4: Artistic representation of a grain boundary [4]. The colored atoms represent the different grains in material and the grey atoms (disordered) represent the grain boundary.

The grain boundary interfaces are generally unstable and the atoms reorder so that the total interfacial energy is minimized. The larger grains grow at the expense of smaller grains so as to reduce the total free energy by reducing the overall grain boundary area. This causes an increase in the average grain size and is referred to ‘grain growth’. Grain growth is an important phenomenon in NC materials and restricting grain growth is one of the important aspects because larger grain size of the material implies a reduction in the yield strength (Hall-Petch effect). The rise of atomistic simulations helped to envision grain boundaries and grain growth in a more articulate way.

Grain growth is accompanied by grain boundary motion. The impact of grain boundary motion increases with temperature and by the application of external

forces. Cahn et al. [38] conducted a study on shear deformation on different grain boundary structures of Cu at high temperatures. They observed that this shear deformation causes both sliding and migration of GB.

2.3 Zener Pinning

Restricting grain growth or grain boundary motion can be useful in maintaining the strength of NC material as discussed above. Adding particles in a NC material can obstruct the grain boundary motion. This gives rise to a new mechanism called Zener pinning [9]. Zener pinning is the effect of adding particles to restrict the grain boundary motion by providing an additional pinning force on the GB. Zener proposed that normal grain growth would be inhibited when the grain size reaches a critical maximum grain radius which is given by

$$R_c = \frac{4r}{3f}, \quad (2.2)$$

where f is the volume fraction of particles, r is the inter-particle spacing.

Several changes were made to the above formulation based on its applicability to realistic situations [39–41]. Manohar et al. [42] reviewed the modifications made to the Zener equation over the past five decades. Based on several research studies, the pinning of particles to the grain boundaries is estimated to depend on a several factors such as: a) shape of particle b) inter-particle distance c) coherency of the particle with the grains d) type of grain boundary e) orientation of grain boundary with the particle f) temperature g) shape of the grains h) distribution of particles i) particle volume fraction. Manohar et al. [42] also indicated that the previous modifications in the calculation of minimum particle size approve a particle radius which is required to hinder grain growth is much higher than the Zener

estimate. The Zener formula in equation 2.2 can be generalized as

$$R_c = \frac{Kr}{f^m}, \quad (2.3)$$

where K is a dimensionless constant and m is an index for f .

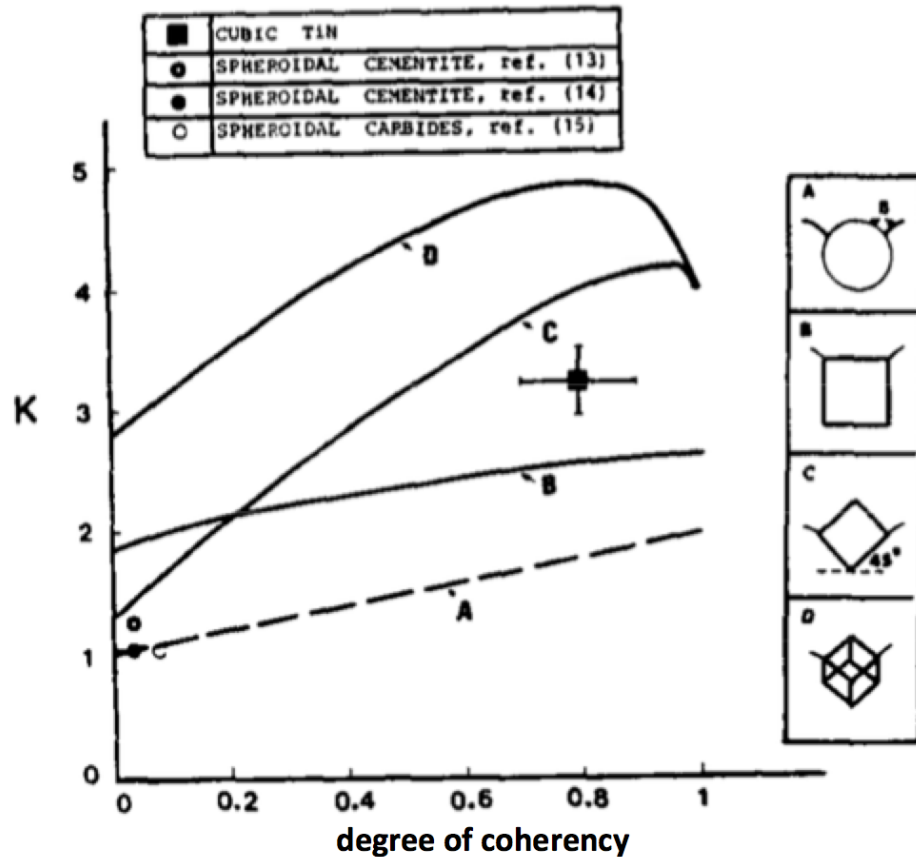


Figure 2.5: Effect of coherency of different types of particle on efficiency of pinning [5]. The pinning force depends on the constant K .

In 1988, Ringer, et al. [5] studied experimentally, the interaction and pinning of grain boundaries by cubic shaped particles. They assess that cubic particles exert a pinning force that is much higher than a spherical particle of the same size. The pinning force that a cubic particle exerts on the grain boundary is almost twice as that exerted by a spherical particle of same size. Figure 2.5 represents the plots of spherical and cubic particles on their effect on the value of K . The pinning force

also depends on the orientation of the cubic particles w.r.t. grain boundary as seen in the figure.

Chen et al. [43] studied the effect of pinning particles on the grain boundary motion using MD. They performed several simulations for different sizes of pinning particles to elucidate their effect on hindering the grain boundary motion. They discuss the importance of GB migration in NC materials and also explore the Brownian motion of the pinned GB.

2.4 Particle Reinforced Nanocomposites

Metal matrix composites (MMCs) are materials with metals as matrix material. Metal matrix composites are significantly used in the field of aerospace and automobile industries due to their high stiffness to weight ratio.

According to Drucker [11], the strength of a two-phase composite does not show a significant increase till the volume fraction of the reinforcement particles in the matrix material increases to a threshold value of about 30%. This is due to the assumed elastic-plastic response of the ductile matrix material in this model. Although the effect of adding brittle particles to a ductile matrix was studied rigorously w.r.t. volume fraction of the composites, there were no detailed calculations explaining the effect of size and shape of reinforced particles. In continuum models, the size and shape of the particles are known to have a negligible effect on the strength of the material. Christman et al. [44] discussed numerically and experimentally, the possible reasons for the increase in strength of MMCs. They suggested that an increase in the composite strength may be generally attributed to a) load transfer between the particles and matrix, b) changes in dislocation density, or c) generation of residual stresses.

G. Bao et al. [6, 45] studied the role of non deforming particles in reinforcing ductile matrix materials against plastic flow and creep using finite element analysis.

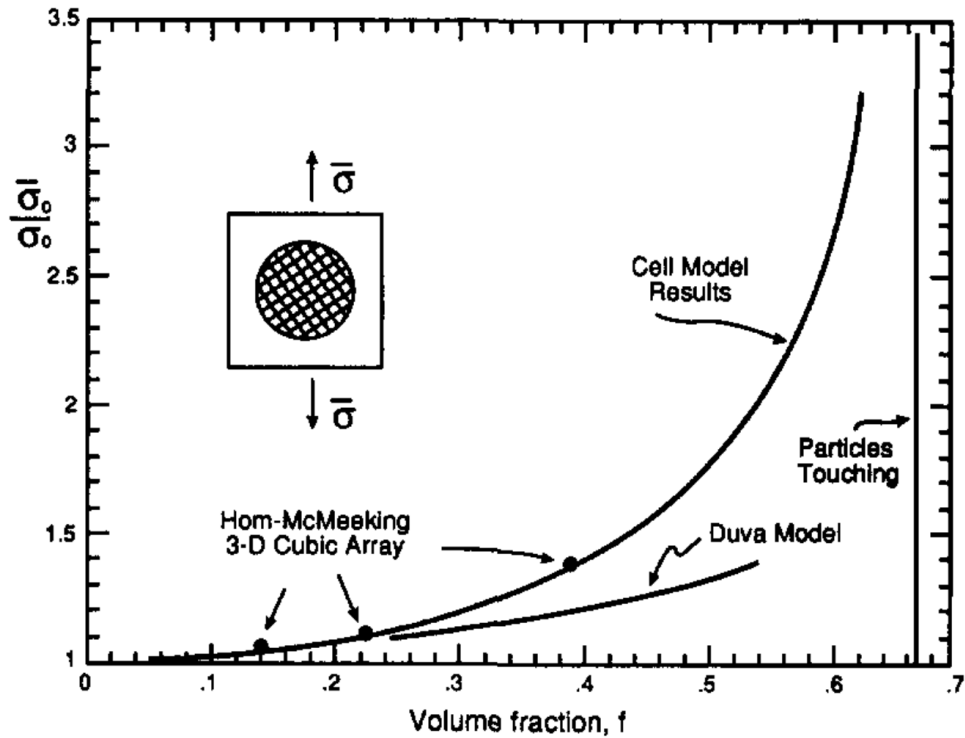


Figure 2.6: Effect of volume fraction of spherical particles on normalized yield strength in ductile metal matrix composites [6].

The study in this paper deals with the uniaxial stress-strain behavior in rate dependent plastic flow of materials or steady-state creep for composites with matrices reinforced by particles which are large enough to justify the continuum plasticity representation of matrix material. Calculations of plastic flow stress and asymptotic reference stress of composites with both elliptical and spherical particles show that these stresses show an exponential relationship with volume fraction of particles. The effect of adding second phase particles to materials has proven to produce composites with enhanced strength. Due to their high stiffness to weight ratio, these metal matrix composites (MMCs) are used in a wide range of applications such as aerospace, and automotive applications [46]. Numerous studies were conducted to examine the mechanical properties of particle-reinforced metal matrix composites [10, 47–49]. They found that yield strength differs by a very less

amount with a change in volume fraction and particle size. They found that both the particle size and volume fraction affect on the strength of these composites. The effect of particle size on the yield strength in case of MMCs is very less when compared to that of volume fraction.

The nano-sized MMCs are called as MMNCs. NC materials already have a high strength when compared to coarse-grained materials and adding particles in NC particles would further increase their strength. Substantial research was done to understand the properties and mechanisms involved in MMNCs [50–52].

Particle size and volume fraction affect the yield strength of MMNCs but they have stronger effects than in MMCs. Particle size is a huge factor affecting the yield strength of MMCs unlike MMNCs. This is because of the presence of additional strengthening mechanisms in MMNCs which are not common in the case of MMCs [50, 53].

Scanlon et al. [54] performed an indentation cracking experiment on metal-ceramic nanocomposites. They found that the hardness of the nanocomposites did not show significant change with increase in volume fraction of the harder phase until it reaches a value of 50-55% and then increases rapidly with further increase in the volume fraction of the harder phase. The compressive strength of a material has a approximately linear relationship with its hardness [55, 56]. Therefore, a similar relationship of yield strength and volume fraction can be implied. This behavior was found consistent with existing continuum models which deduce yield strengths of different volume fractions of second phase particles but these results were not addressed specifically for nano-scaled microstructures.

CHAPTER 3 COMPUTATIONAL APPROACH

Before the rise of computational modeling of materials, the study of nanomaterials was done either theoretically or experimentally. Computational modeling investigates the mechanical properties and explores the atomistic deformation. Computational modeling of materials bridges the gap between theory and experiments. In other words, a theory can be tested using a computational model and can be validated using the available experimental data. Another advantage of computational modeling is that it can be used to test a model that is difficult or even impossible to conduct in a laboratory [57].

Molecular Dynamics is used as tool of computational modeling in the simulations performed in this study. All the simulations were performed using LAMMPS [58], a parallel computing molecular dynamics package.

3.1 Molecular Dynamics

Molecular Dynamics is a computational method based on classical, Newtonian mechanics. MD regards the material as a system of N discrete particles/atoms. The interaction between the particles is described by an empirical interaction potential function. The interatomic potential defines how atoms interact by exerting forces on each other. This potential function can be defined by a number of theories.

The interaction potential can be used to find the interaction forces on each particle. These interaction forces are then used either in energy minimization for molecular statics or to solve the equations of motion in molecular dynamics. For N particles in a system, there would be $3N$ equations of motion. By solving these equations, new positions and velocities are obtained for the subsequent timesteps. These simulations when run for a significant time interval under the given boundary

conditions would deduce the different mechanisms involved in the process. Hence, to understand the steps involved in MD, the next few subsections on interatomic potential, interaction force, energy minimization, equations of motion, visualization and limitations of MD are discussed to give a brief overview on MD.

3.1.1 Interatomic Potential

The atoms in the material either repel each other when they are too close or attract each other when they are at larger distances. The forces which cause these attraction or repulsion is defined by a unique function called the interatomic potential. There are two common types of interaction potential, namely pair potential and multi-body potential. A pair potential defines the interaction of each particle with every other particle. An example of pair potential is the LJ potential [59], which is given by

$$\phi(r) = 4\epsilon_0\left[\left(\frac{r}{r_0}\right)^{-12} - \left(\frac{r}{r_0}\right)^{-6}\right], \quad (3.1)$$

where ϵ_0 is the depth of potential well, r_0 is the distance at which the interatomic potential is minimum. The positive and negative terms in the brackets represent the attraction between the atoms which are at a larger distance.

The pair potential determines the interactions of particle i with every other particle, and does not consider the combined effect of particles. The pair potential was thus, extended to a multi-body potential to represent the system more significantly. A multi-body potential such as the embedded atom method (EAM) potential [60] describes the interaction of N particles in a system by

$$\phi(\mathbf{r}_i) = \sum_{i < j} \phi(\mathbf{r}_{ij}) + \sum_i \mathbf{F}\left(\sum_{j \neq i} \rho(\mathbf{r}_{ij})\right), \quad (3.2)$$

where \mathbf{r}_{ij} represents the distance between the particles i and j , $\mathbf{F}(\sum_{j \neq i} \rho(\mathbf{r}_{ij}))$ is the embedding function corresponding to particle i . The widely used interaction

potential for metals is EAM because of its computational efficiency as observed in most of the fcc metals [61, 62].

3.1.2 Interaction Force

The interaction force is defined by the negative gradient of the potential function for a given system. The interaction force on particle j is given by

$$\mathbf{f}_i = -\frac{\partial\phi(\mathbf{r}_j)}{\partial\mathbf{r}_i}, \quad (3.3)$$

where ϕ is the potential function, \mathbf{r}_i represents the atomic position of particle i . These interaction forces are used to solve energy minimization and equations of motion.

3.1.3 Energy Minimization

Energy minimization in MD simulations is done to find the lowest potential energy of the system. Energy minimization is done at static conditions when the kinetic energy of the atoms is ignored (system at zero temperature). When energy is minimized in a system, the interatomic force on the system given by equation 3.3 can be estimated as zero. The basic energy minimization technique is the steepest descent method. The negative gradient of the interatomic potential function as given in equation 3.3 is used as the direction of the fastest direction towards a local minimum. This is not a very efficient energy minimization technique but its a very fast converging algorithm. The most commonly used energy minimization technique is the conjugate gradient method because of its computational efficiency and simplicity [63]. The conjugate gradient uses the derivative of potential function already computed initially for finding the optimal direction, which makes it more efficient than steepest descent method.

3.1.4 Equations of Motion

Based on the initial positions (r_i), velocities (v_i) and forces (f_i), a new atomistic configuration of the system is found by solving the Newton's equation of motion given by

$$f_i = m \cdot a_i = m \cdot \frac{dv_i}{dt} = m \cdot \frac{d^2r_i}{dt^2} = \partial\phi_{r_j}/\partial r_i, \quad (3.4)$$

where $\phi\{r_i\}$ represents the potential energy of system at a given configuration, a_i represents the acceleration. In MD, these equations of motion are solved using Verlet's algorithm which is one of the stable and simplest algorithms. The Verlet algorithm is based on symmetric finite difference approximation for acceleration. For a given time interval, $t_n = n\delta t$, where δt is the timestep and n is the number of timesteps.

3.1.5 Visualization

Using the Newton's law of motion, the atomistic configurations at different times are computed by the Verlet algorithm. These atomic configurations have the positions and velocities of different atoms which are used to visualize the resulting structures. There are different techniques used in finding the defects and the free structure. Some of them are centrosymmetric analysis, common neighbor analysis, and bond angle analysis. The centrosymmetric parameter measures the lattice disorder around an atom, the common neighbor analysis is used to find the structure type of each atom such as fcc, bcc, hcp, or any other lattice and the bond angle analysis is also used to find the structure type but by using the information of the orientation of the bonds of a particular atom with the neighboring atoms. These tools can be used to find the atomistic deformation in the structure and hence, can be used to find yield point of a material by observing the plastic deformation in the structure.

The output files of LAMMPS can be used to find the atomic configurations of a system at different time intervals. These atomic configurations can be visualized using these tools provided in a visualization software such as OVITO [64].

3.1.6 Limitations

Though MD is an exceptional tool to observe the atomistic deformations within a system under different conditions, it has quite a few limitations [65–67]. Firstly, as MD is based on solving Newton's equations of motion, quantum mechanical effects are neglected and hence, by not considering the Schrodinger's equation, a significant simplification is made at very low temperatures where electronic calculations are important.

MD relies significantly on the potential function and the atomic force fields which defines the physical model are derived from this potential function. Hence, the results of these simulations would be realistic only if the potential function used can derive accurate force fields on the atoms. Another issue with the potential function is that these functions should have a simple functional form to reduce the computational time. Also, these potentials should be applicable to many systems under different conditions. Hence, developing these potentials is a challenging task.

Using MD, one can observe the defects in nanomaterials with ease but the nano-level timescales and lengthscales used in MD are not the same as used in experiments. Hence, large systems of micrometer size cannot be investigated as MD is limited only to nano-sized structures. Also, as the timescales and lengthscales involved are very low, the simulations which involve mechanisms such as creep and diffusion are impractical to observe in classical MD. However, ongoing research on increasing these timescales with the evolution of techniques such

as Autonomous Basin Climbing (ABC) assure the material modeling scientists to reach higher timescales.

CHAPTER 4 ZENER PINNING

4.1 Introduction

As discussed earlier, every material is made of large number of grains which are a group of atoms with a perfect crystal lattice. In nanomaterials, the grain size is of the order of nanoscale, hence, nanomaterials have a large number of grains with different orientations of atoms. Grain boundary is the transition region between any two differently oriented grains. The atoms in this region have a different orientation as any of the two adjacent grains. Grain boundaries impart strength by being effective barriers to dislocation motion.

4.1.1 Zener Pinning

NC material have attained more attention because of their high mechanical strength. This high mechanical strength is due to the presence of large number of GBs in unit volume of NC material. As discussed earlier in chapter 2, grain growth is one of the important phenomena in to be hindered for a NC material to maintain its high strength. Grain growth is common at elevated temperatures and sometimes, even at low temperatures. One way to prevent the GB motion is by Zener pinning. Zener pinning is a mechanism of adding second phase particles into the NC material so that these particles provide a pinning force that make the GBs difficult to pass through them.

The atomistic simulations of Zener pinning would give an idea on how the GB motion can be restricted. The effect of particle size, and inter-particle spacing is discussed in this chapter. Before discussing the methodology of the simulations performed, an attempt to understand GB motion is made in the next subsection.

4.1.2 Grain Boundary Motion

As grain growth is directly related to GB motion, the importance of restricting GB motion is already discussed previously. GB motion is mainly caused either by an increase in temperature of material or by application of external forces. The different types of grain boundary motion are:

1. sliding: movement of grain boundary in a direction parallel to its plane.
2. migration: movement of grain boundary in a direction normal to its plane.

At high temperatures, as grain boundary motion is common, the effect of shear on NC bicrystals at high temperatures is studied in this chapter. The methodology of the study is explained in the next section.

4.2 Simulation Methodology

To study the effect of Zener pinning, atomistic simulations were performed on Cu. High temperature was chosen in this study as the grain boundary mobility at high temperatures is significant [38]. Two types of grain boundaries were studied with $\Sigma 5(310)$ and $\Sigma 17(410)$ symmetrical $[0\ 0\ 1]$ tilt GBs. $\Sigma 5$ is a high-angle GB with a tilt angle of 36.87° while $\Sigma 17$ is a low-angle grain boundary with a tilt angle of 28.07° . All the simulations were performed using LAMMPS [58].

The GB specimens used in this study were created using Mark Tschopp's code [68, 69]. These specimens were generated by creating two separate crystals, crystal 1 and crystal 2 of different orientations which are placed in such a way that they form a bicrystal. The overlapping atoms are deleted and energy minimization is performed to create the required grain boundary specimens. In the case of $\Sigma 5$, the orientations of crystal 1 are $x(3\ 1\ 0)$, $y(-1\ 3\ 0)$, $z(0\ 0\ 1)$ and that of crystal 2 are $x(3\ -1\ 0)$, $y(1\ 3\ 0)$, $z(0\ 0\ 1)$. The $\Sigma 17$ bicrystal is generated in a similar fashion. The bicrystals generated corresponding to $\Sigma 5$ and $\Sigma 17$ are

named as X and Y respectively. The number of atoms in these bicrystals were around 10^4 atoms. Table 4.1 gives the description of specimens planned to study in this chapter. The description of the specimens generated to study the shear are tabulated in table 4.1. X0 and Y0 represent the specimens with no particles. H represents the height of the specimen in angstroms. The sizes of the specimen types X and Y were $90 \text{ \AA} \times 113 \text{ \AA} \times 14.4 \text{ \AA}$ and $90 \text{ \AA} \times 120 \text{ \AA} \times 14.4 \text{ \AA}$ in the x, y, and z directions respectively. As both the bicrystals have the same length in the X direction, the number of particles in contact with unit GB area was constant. The inter-particle spacing in both the specimens was approximately equal to 90 \AA as periodic boundary conditions were implemented to the bicrystals.

Table 4.1: Different particle diameters used to study Zener pinning in sigma 17 grain boundary

Specimen	# of atoms	# of particles	Particle diameter (in nm)
X0	12672	0	n/a
X1	12672	1	4.4
Y0	12960	0	n/a
Y1	12960	1	4.4
Y2	12960	1	6.2
Y3	12960	2	4.4

To study the effect of shear on grain boundary motion, a high temperature of 800 K was chosen. The EAM potential of Cu by Mishin et al. [70] was used. Periodic boundary conditions were implemented for the bicrystals in all the simulations. The strain rate chosen in all the simulations was around 10^8 s^{-1} , which lies in the MD range. The simulations with particles in the specimen types X and Y were performed after studying the effect of shear on grain boundary motion when no particles were present. Initially, each specimen was divided into three regions: a) upper, b) lower, and c) mobile as shown in the figure 4.2. The ‘lower’ region was kept fixed and the shear was applied on the ‘upper’ region. The atoms in the ‘mobile’ region are free to move without any restrictions. Microcanonical ensemble

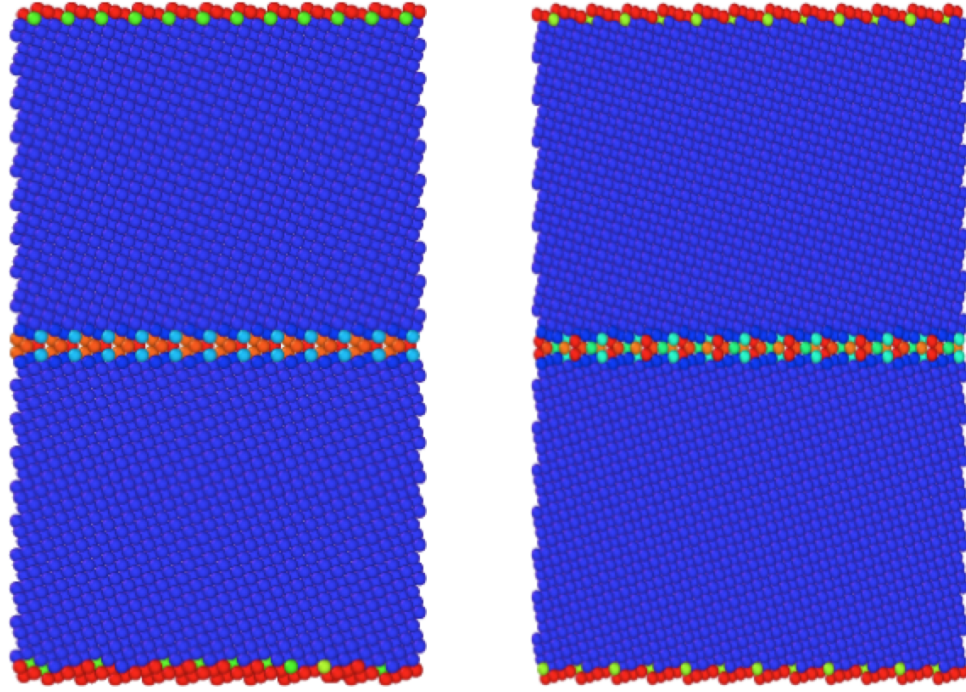


Figure 4.1: Σ 5 and Σ 17 grain boundaries generated using LAMMPS. The number of atoms in both the specimens were around 10,000.

(NVE) was used in all the simulations. The grain boundary motion was visualized using OVITO [64]. The stress-strain plots were obtained from the LAMMPS output files. GB Displacement-time curves were plotted to observe the effect of shear on grain boundary motion.

To study the effect of shear on specimens with/without particles, different specimens were generated to study Zener pinning. The different specimens used to study the shear deformation are tabulated in table 4.1. The specimens X0 and Y0 do not have particles in them and shear was applied to study the displacement-time variation and stress-strain analysis to observe the GB trends in these specimens. The direction of GB motion was initially observed in the specimens X0 and Y0. Different specimens were created of types X and Y with particles to study the effect of Zener pinning. These cylindrical regions act as particles and were treated as rigid in all the simulations. The particles were placed in the crystal towards which



Figure 4.2: Different regions defined in the GB specimens. The lower region was held fixed and shear was applied on the upper region.

the GB tends to move in the corresponding specimen types. All the particles were placed at a distance of 8.5 Å from the center of the bicrystal to observe the grain boundary motion before the GB pinning is observed. The shear simulations were then performed again on the specimens with particles.

4.3 Results and Discussion

The specimens X0 and Y0 have grain boundary energies of 0.905 J/m^2 and 0.915 J/m^2 , which are very close to the results of Cahn et al. [38]. The stress-strain curves and displacement time curves of specimens X0 and Y0 as shown in figures 4.3 and 4.4 are also consistent with Cahn et al. The continuous fluctuations in the stresses represent the stick and slip behavior of the GB and the sudden drop in the stresses at few points represent the GB migration. These plots indicate that $\Sigma 17$ displaced by about 15 Å in 1 ns whereas the displacement of $\Sigma 5$ is only

about 10 Å in 1 ns. This indicates that the GB motion in case of Σ 17 is more than that in the case of Σ 5 for the same applied stress.

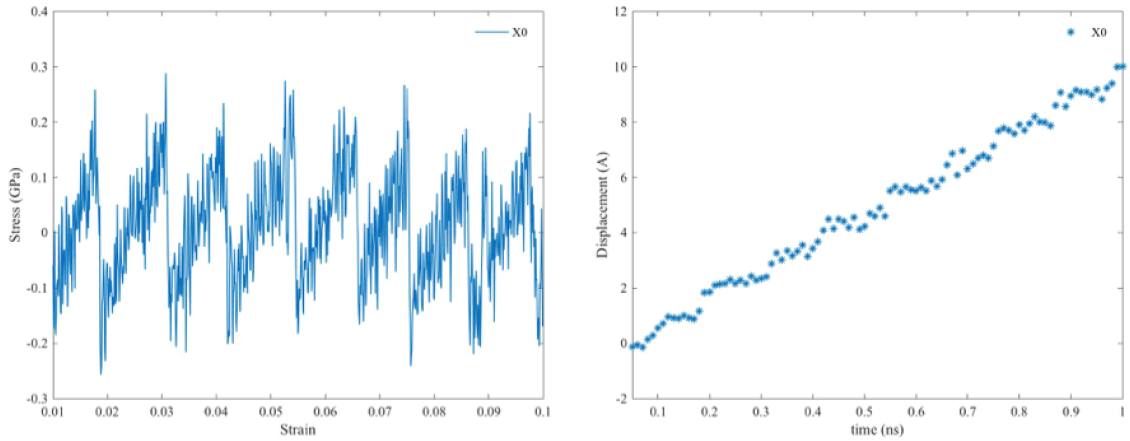


Figure 4.3: Stress-strain and displacement-time curves of specimen X0 at 800 K with a shear velocity of 1 m/s.

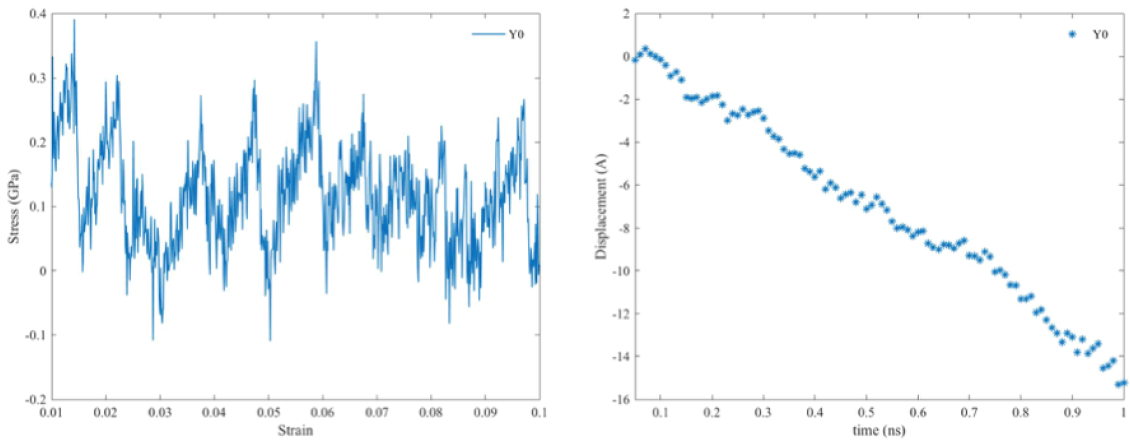


Figure 4.4: Stress-strain and Displacement time curves of specimen Y0 at 800 K with a shear velocity of 1 m/s.

Figures 4.5 and 4.7 represent the stress-strain curves of specimens X1 and Y1 respectively. The particle size is 4.4 Å in these bicrystals. In both the specimens, a displacement of about 7 Å (distance from center of bicrystal to the particle boundary) was needed for the GB to make a contact with the particle. For this displacement, strains of 0.07 and 0.05 were required in specimens X0 and Y0. The plots of specimens X1 and Y1 also show that until the specimens were strained to

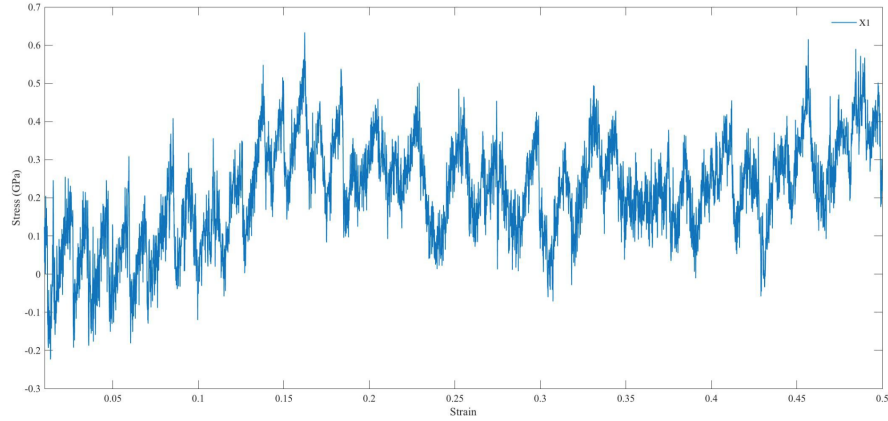


Figure 4.5: Stress-strain curve of specimen X1 at 800 K with a shear velocity of 1 m/s. Particle diameter = 4.4 Å.

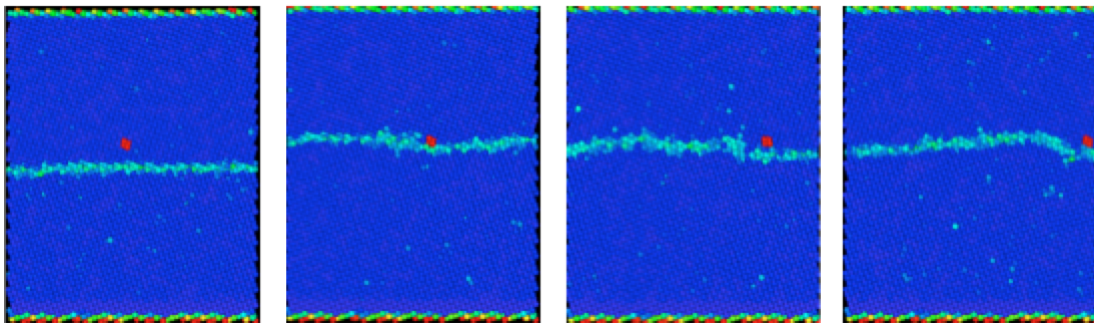


Figure 4.6: Visualizations of Σ 5 tilt GB under shear strain. The pinning pressure provided by the particle counteracts the driving force of GB and this is a case of efficient pinning as GB motion is hindered.

0.07 and 0.05 respectively, the stress-strain curves look similar to those in specimens X0 and Y0.

Figures 4.6 and 4.8 display the visualizations of specimens X1 and Y1 respectively. In both the cases, the GB moves towards the particle initially. In specimen X1, efficient pinning is observed as the GB does not detach from the particle even after 5 ns. In specimen Y1, the pinning is not as efficient as it is observed in specimen X1. The Σ 17 GB detaches from the particle at a time of 1 ns. The probable reason for the different scenarios observed in these two cases may be the difference in the velocities of GB migration of the two GBs as observed earlier in specimens X0 and Y0 (figures 4.4 and 4.3).

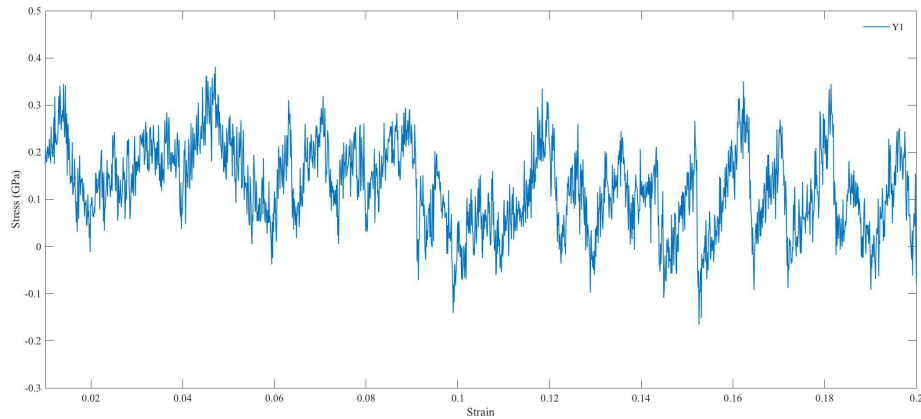


Figure 4.7: Stress-strain curve of specimen Y1 at 800 K with a shear velocity of 1 m/s. Particle diameter = 4.4 Å.

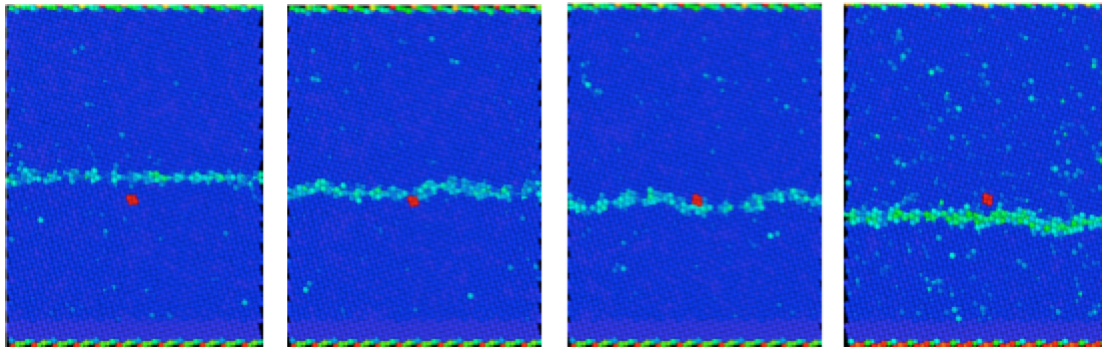


Figure 4.8: Visualizations of $\Sigma 17$ tilt GB under shear strain. The driving force of GB is higher than the pinning force provided by the particle. Pinning is not as efficient as observed in $\Sigma 5$ tilt GB.

The results of specimen Y1 indicate that a shear stress of about 0.4 GPa was sufficient for the GB to unpin from the particle. This is quite low when compared to the case of specimen X1 where a shear stress of 0.6 GPa could not unpin the GB from the particle. Figure 4.9 represents the stress-strain plot of specimen Y2. The particle size is increased by about 2 Å. As seen in the figure, the shear stress values reaches a maximum of about 1 GPa but pinning is not observed in this case. The saw tooth behavior observed in this plot is more noticeable because of the strong pinning force applied by the particle. This shows that a significantly high pinning force is applied by increasing the particle size by just 2 Å.

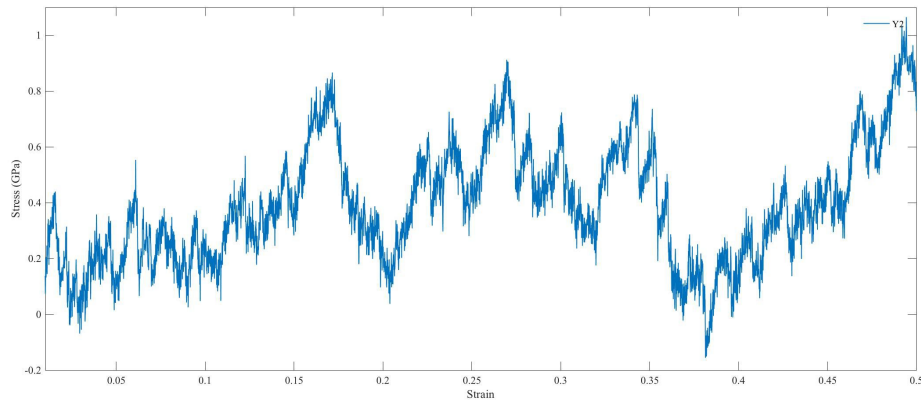


Figure 4.9: Stress-strain curve of specimen Y2 at 800 K with a shear velocity of 1 m/s. Particle diameter = 6.2 Å.

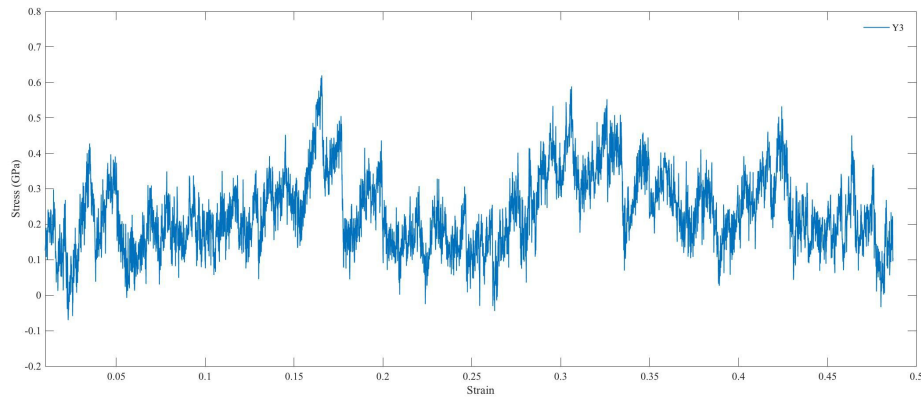


Figure 4.10: Stress-strain curve of specimen Y3 at 800 K with a shear velocity of 1 m/s. Particle diameter = 4.4 Å.

The stress-strain plot of specimen Y3 is displayed in figure 4.10. As seen, the trend in the plots suggests that the pinning force applied by two particles of 4.4 Å diameter is less effective when compared to one particle of 6.2 Å diameter.

4.4 Conclusion

The following observations were made from the atomistic simulations on GB specimens Σ 5 and Σ 17:

1. The GB specimens show a saw tooth behavior consistent with Cahn et al.'s results [38]. The displacement-time curves indicate that Σ 17 displaces by 5 Å more than that of Σ 5 in 1 ns time. A shear stress of just 0.3 GPa on the GB specimens at 800 K was sufficient for GB migration to occur.
2. The effect of pinning can be increased by increasing the particle diameter, or by increasing the number of particles in the specimen. Increasing the particle size by just 2 Å has significantly larger pinning effect on the GB. A shear stress of 1 GPa could not unpin the Σ 17 GB.
3. The pinning effect observed by increasing the particle size is greater than that of increasing the number of particles per unit GB area. As cylindrical particles were used, the effect of Zener pinning by increasing the diameter is very high.

CHAPTER 5 PARTICLE REINFORCED NANOCOMPOSITES

5.1 Introduction

As discussed in Chapter 2, grain growth is one of the important phenomena in achieving materials with better mechanical properties. Restricting the grain boundary motion leads to grain boundary stability and hence larger forces would be required to undergo plastic deformation in the material. The impact of adding second phase particles to restrict the grain boundary migration was discussed in chapter 4. The volume fraction of particles considered in chapter 4 was around 0.2% which is not very high but the impact of these particles in restricting the grain boundary was clearly evident. By intuition, one can easily hint that increasing the volume fraction of particles to about 50% would provide nanocomposites of remarkable mechanical properties because the particles not only restrict grain boundary motion but also add strength to the composites. In this chapter, the impact of adding high volume fraction of particles (up to 50%) on the mechanical properties of nanocomposites is discussed. High particle volume fraction is generally used

The composites which have metals as matrix material are generally referred as metal matrix composites (MMCs) and these materials in nano-level are called as metal matrix nanocomposites (MMNCs). The composites used to study in this chapter are MMNCs. Before exploring the methodology of the study, a brief overview on MMNCs and an outline of strengthening mechanisms in nanocomposites are discussed.

5.1.1 Metal Matrix Nanocomposites (MMNCs)

In producing ultrahigh strength materials, ductility is incompatible as it might lead to a catastrophic failure as ductile materials are generally soft. However, if the material is highly brittle, enormously high elastic stress concentrations in at least

small regions of the material are observed during the fabrication process. Hence, little ductility can eliminate these stress concentrations. A mix of ductile matrix with brittle particles can be used to provide these ultrahigh strength materials [11].

There has been significant research on MMCs and MMNCs recently. Bao et al.'s study [45] indicates that volume fraction has an exponential relationship with the yield strength of MMCs. This relationship was also observed in the experimental results of Scanlon et al. [54] where nanocomposites of $Ag - Al_2O_3$ and $Fe - SiO_2$ were investigated. In both the cases, the volume fraction has a very weak effect on the yield strength until a threshold value of 30% volume fraction of particles is reached. After the threshold value, the volume fraction of particles has a very strong effect on the yield strength of composites. This surprising relationship which is common in both continuum and nano levels is the main motivation for the study in this chapter. The main objective in this chapter is to check the validity of the existing continuum models at nano-level.

5.1.2 Common strengthening mechanisms in MMNCs

Before proceeding to analyze the yield strength of nanocomposites at different volume fractions, the various strengthening mechanisms involved in nanocomposites that were studied earlier are discussed as follows:

1. Load bearing effect: At nano-size, a strong cohesion between matrix and reinforcement particles is attained. This strong cohesion occurs at atomic level and hence, the nano-sized particles are directly bonded to the matrix [71, 72]. The nano-sized particles would carry a fraction of load which gives rise to a load transfer between matrix and reinforcement [50]. The expression for the improvement factor f_1 associated for load bearing effect is given by

$$f_1 = 0.5 \times f, \quad (5.1)$$

where, f is the volume fraction of particles in the nanocomposites. The above equation is valid if the material is assumed to have negligible porosity.

2. Orowan strengthening: Orowan strengthening is caused by the resistance of closely spaced particles to the passing of dislocations [53]. Orowan strengthening is not observed in micro-sized MMCs but it is widely common in MMNCs, particularly when the inter-particle distance is less than 100 nm. Orowan strengthening is inversely proportional to the inter-particle distance and hence, this strengthening effect is significantly larger in the MMNCs with smaller particles. Hence, for the same particle volume fraction of particles in the matrix material, the composites with smaller particle sizes have smaller inter-particle distance and higher strengthening effect.
3. Enhanced dislocation density strengthening mechanism: Nano-sized particles in MMNCs have higher interfacial area between the reinforcement and matrix materials. This leads to enhanced mechanical properties. The thermal mismatch of reinforcement and matrix materials when the materials are processed when brought to equilibrium leads to the development of thermal stresses within the material at the interface between. These stresses are large enough to cause plastic deformation in the matrix and can cause to form a high dislocation density at the interface. The strengthening effect is directly proportional to: a) difference in processing and test temperatures b) difference in thermal coefficient of the two phases of the composite. However, if the yield strength of the nanocomposite is tested at processing temperature, the strengthening caused by this mechanism is zero.

5.2 Simulation Methodology

To study the high particle volume fraction nanocomposites, silver was used as matrix material and rigid particles were used. Silver is chosen because of its excel-

lent ductility. When rigid particles are present in the ductile silver matrix, these high volume fraction particles in the composite provides the desired ultrahigh strength. and the ductility of the matrix material would ensure that there would not be any extremely high elastic stress concentrations at the interphase. To compare the results of these nanocomposites, existing elasto-plastic models presented in Bao et al.'s paper [45] are used. The choice of silver in this study is not only motivated because of its high ductility but also its vital use in the field of nanotechnology especially in drug delivery, agriculture, and electronics [73–83].

Atomistic simulations were performed to study the effect of high particle volume fraction on mechanical properties of MMNCs. All the simulations were performed using a molecular dynamics package, LAMMPS [58]. The material used was Ag and Embedded Atom Method (EAM) potential developed by PL Williams, Y Mishin and JC Hamilton [84] was used. Ag polycrystals were made using Voronoi tessellations of Ag single crystal and were created using the utilities provided by J.Li [85]. Two specimen sizes were used in this study to elaborate the effect of particle size by keeping the volume fraction constant. A, B and C represent the specimen types with sizes 24.6 nm, 36.9 nm, and 49.2 nm respectively. The number of atoms in the specimens was varied from around 800,000 atoms to 6.7 million atoms. The grain size used in the simulations was about 12.3nm. The small grain size was chosen to make it consistent with the available experimental data provided by Scanlon et al. [54]. The grains in the polycrystals have the shape of truncated octahedrons and have random orientations. The number of grains in the specimens vary according to the respective size of the specimens. The description of the two specimen types was tabulated in table 5.1.

Cubic particles were used as simulations of specimens with volume fractions more than 50% of particles were desired. If spherical particles were used, the maximum volume fraction of particles that could be reached was about 50% in which

Table 5.1: Description of different specimen types used in this study

Type	Size (in nm)	# of atoms	# of grains
A	24.6	827,774	16
B	36.9	2,794,238	52
C	49.2	6,622,192	108

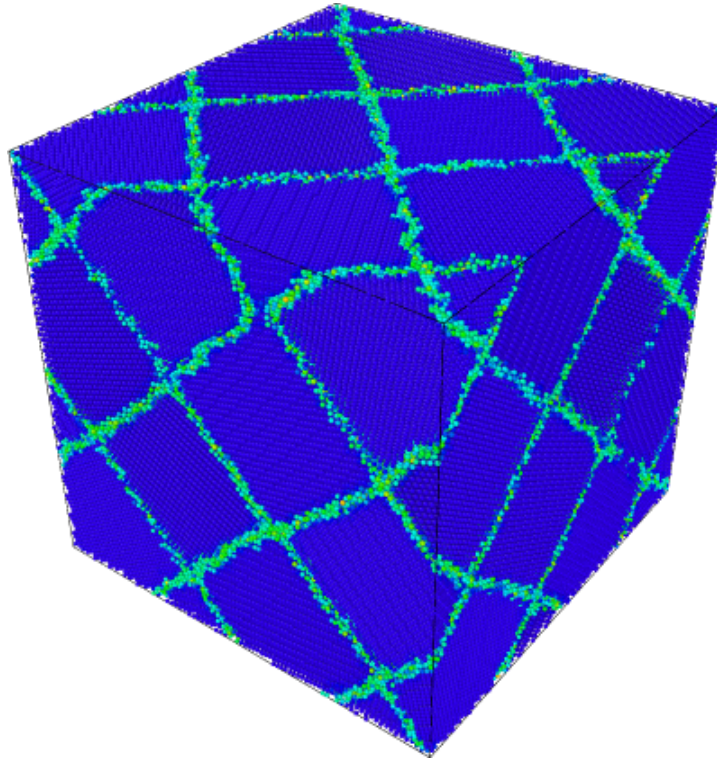


Figure 5.1: Visual of Specimen A0 as seen in OVITO. The number of atoms in the specimen was 827,774.

the particles would be almost adjacent to each other and hence have a negligible inter-particle spacing leading to very high stress concentration in this region. Five particle volume fractions were used: 10%, 20%, 30%, 40%, and 50%. The description of the specimens with particles were tabulated in tables 5.2, 5.3 and 5.4. The particle sizes used in this study vary from 10 nm to 40 nm. The calculations of particle size and inter-particle spacing for each specimen was explained in detail in appendix (A). All the specimens except A0, B0 and C0 have 1 particle in them. Thus, specimen types A, B and C have different packing fractions, which is defined

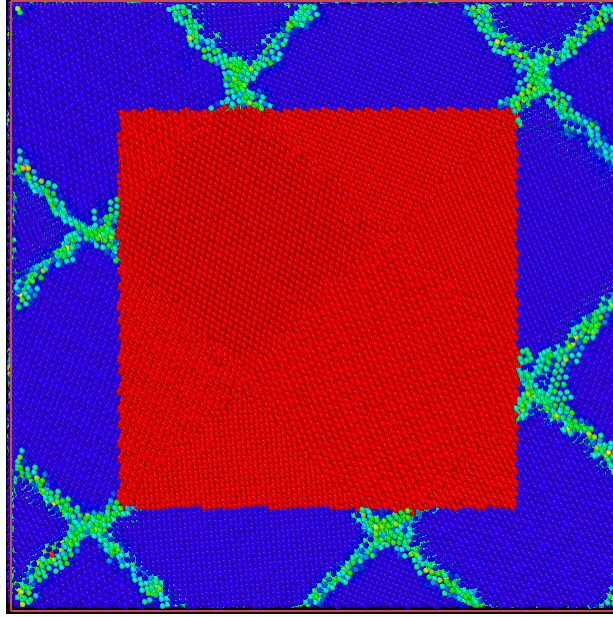


Figure 5.2: Deformation of specimen A3 under a compression strain. The strain rate used was $5 \times 10^8 \text{ s}^{-1}$.

as the number of particles per unit volume and the volume fraction of particles were differed. Figure 5.2 displays the visual of cross-section (X-Y) of specimen A3 as observed in OVITO [64]. The blue region represents fcc atoms (Ag), the green regions represent the grain boundaries and the red region represents the rigid particle.

Table 5.2: List of specimens of type A.

Specimen	vol%	# of particles	d in nm	r in nm
A0	0%	0	n/a	n/a
A1	10%	1	11.5	13.1
A2	20%	1	14.5	10.1
A3	30%	1	16.5	8.1
A4	40%	1	18.2	6.4
A5	50%	1	19.6	5.0

Compression tests of these specimens under periodic boundary conditions were performed to find the yield strength. The potential energy was initially minimized using the conjugate gradient method and then the system was thermally

Table 5.3: List of specimens of type B.

Specimen	vol%	# of particles	d in nm	r in nm
B0	0%	0	n/a	n/a
B1	10%	1	17.0	19.9
B2	20%	1	21.4	15.5
B3	30%	1	24.5	12.4
B4	40%	1	27.0	9.9
B5	50%	1	29.0	7.9

Table 5.4: List of specimens of type C.

Specimen	vol%	# of particles	d in nm	r in nm
C0	0%	0	n/a	n/a
C4	40%	1	36.4	12.8
C5	50%	1	39.2	10.0

equilibrated at near-zero temperature for 50ps using NPT ensemble. The particles were considered rigid and hence, undergo zero deformation. All the particle-matrix interfaces were perfectly coherent to the grains to the structure as a region within the polycrystal was designed as rigid. The compression strain rate used in all the simulations was $5 \times 10^8 s^{-1}$ in the Y direction. The simulations were carried out until the specimens undergo significant plastic deformation. The deformation in the structure was observed by tracking the defects in the specimens with common neighbor analysis tool provided in OVITO [64]. The stress-strain curves were plotted using LAMMPS [58] output files. The yield point was found by using stress-strain curves and OVITO visualizations.

5.3 Results and Discussion

The simulations with specimen A0 approved that compressive yield strength of Ag polycrystal was 1.1 GPa. The Youngs modulus of Ag was around 30 GPa. These mechanical properties seem convincing when compared to the in-situ ex-

periments of NC Ag [86, 87]. The yield point is observed at a strain of 3.9%. The snapshots of the X-Y cross section of specimen A0 at different strains are displayed in figure 5.3. These simulations were first tested with atomistic simulations of Cu specimens performed by Van Swygenhoven et al. [27] and the results were consistent with the approach adopted in this work.

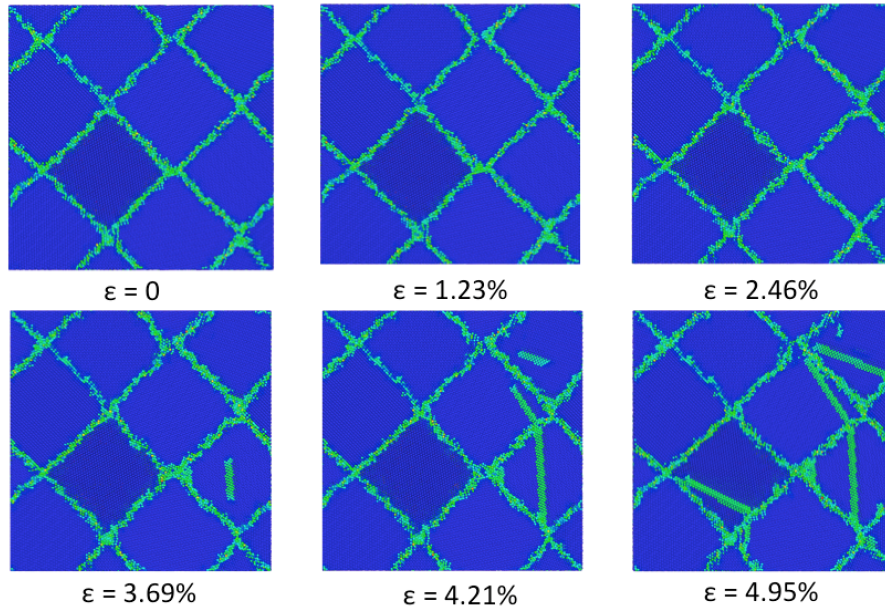


Figure 5.3: Snapshots of specimen A0 at different strains. The yield point was observed at a strain of about 3.69%.

The simulations of specimens with particles (A1-A5) suggested that the yield point of the nanocomposites occurs at a very less strain compared to specimen A0. Figure 5.4 shows the visualization of specimen A3 at different strains. The yield point of specimen A3 occurs at 1.46% strain which is very less than 3.9% strain corresponding to yield point of specimen A0.

Figure 5.5 displays the stress-strain curves of specimens with different particle volume fractions. These curves suggest an increase in the yield point of nanocomposites with an increase in volume fraction when the packing fraction of the specimens is kept constant.

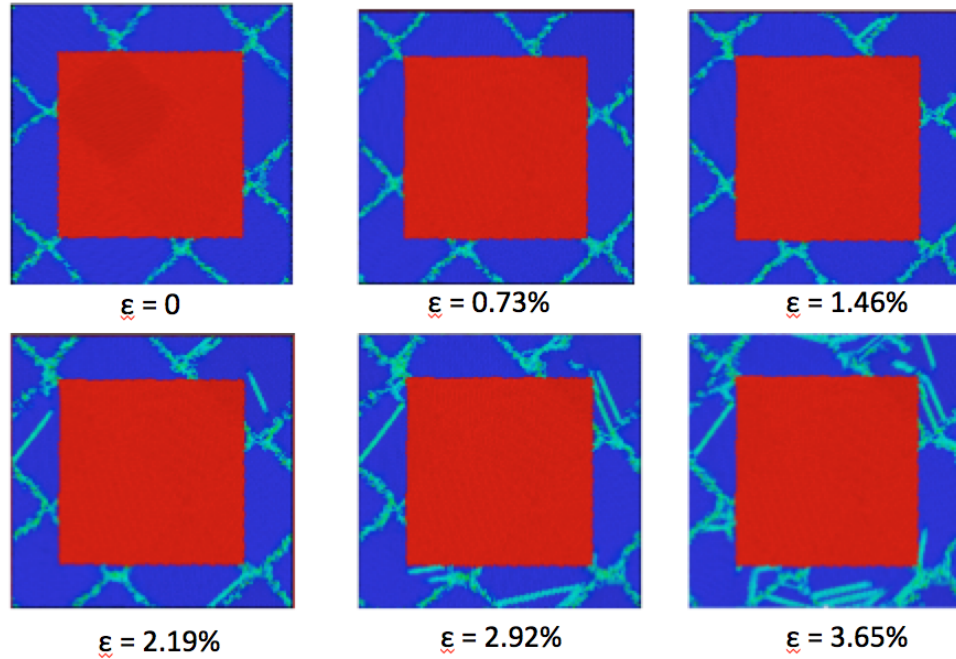


Figure 5.4: Snapshots of specimen A3 at different strains. The yield point was observed at a strain of about 1.8%.

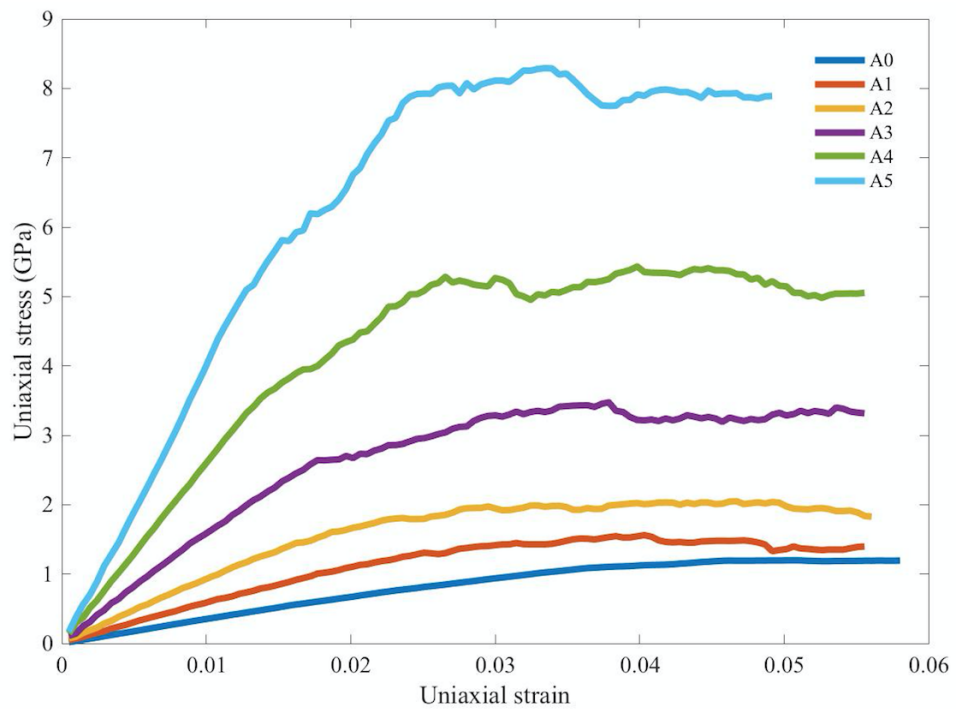


Figure 5.5: Effect of volume fraction on stress-strain curves of different specimens of type A.

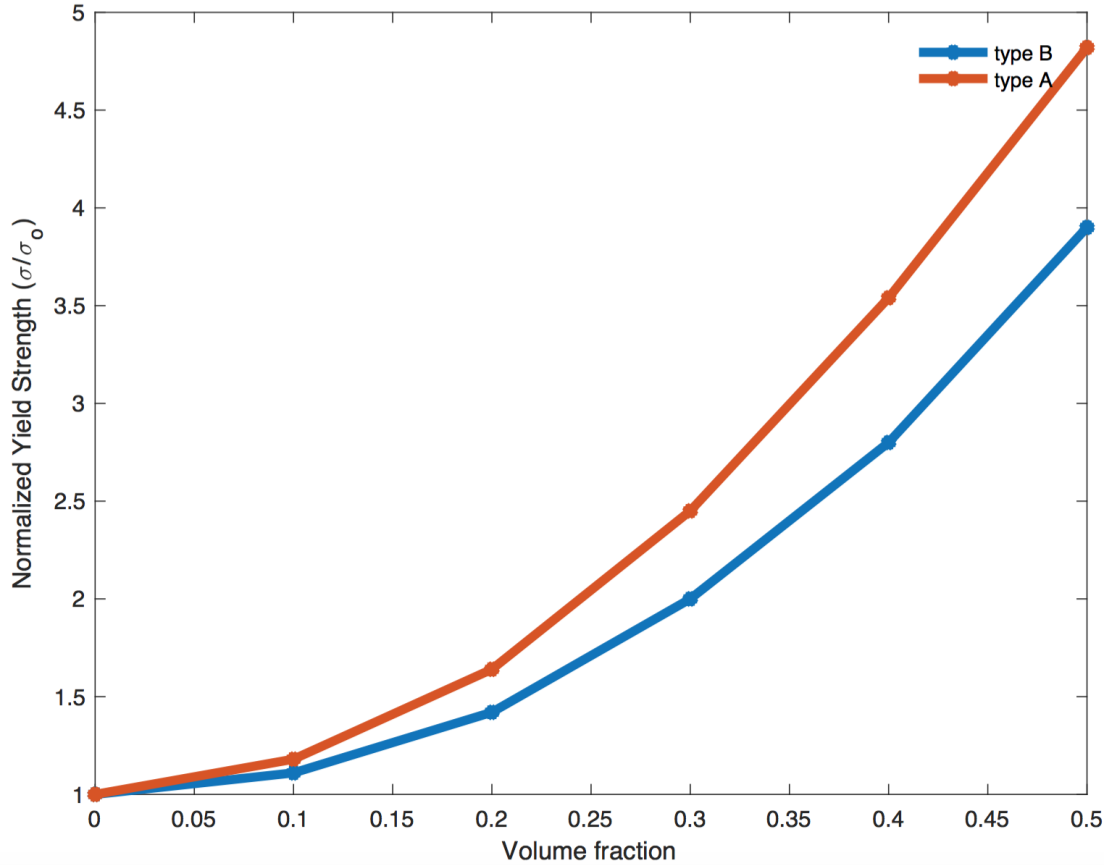


Figure 5.6: Effect of volume fraction on normalized yield strength of different specimen types.

Figure 5.6 displays the effect of volume fraction on normalized yield strength for different specimen types. Normalized yield strength is defined as the ratio of yield strength of specimen with particle w.r.t. yield strength of specimen without particles. As periodic boundary conditions were implemented to study the compression of Ag polycrystals and the strain rate was kept constant in all the simulations, the yield strength of specimens A0, B0 and C0 were roughly equal. As seen in the figure, type A specimens have slightly higher yield strength when compared to type B specimens. This is because the type A specimens have smaller particle size and inter-particle distance compared to type B specimens. Another observation in this figure is that as the volume fraction increases the difference between the normalized yield strengths of the two specimens increases. These simula-

tions if extended to even bigger specimen sizes, say few micrometers (which is not possible in LAMMPS) would reveal the properties of micro-scaled composites and would not show much effect on the particle size of the composites. The yield strength increases to about 5 times when the particle volume fraction of the particles is increased to 50%. This tremendous effect may not be seen in the case of MMCs and the yield strength may increase only up to 2 times when the volume fraction increases to 50% of the MMC [45]. Hence, in coarse-grained composites, the volume fraction has a smaller effect on the yield strength when compared to their nanocomposites counterparts. A notable remark in this analysis is that even though the yield strength of nanocomposites varies with volume fraction in a qualitatively consistent way, the nano-size of the particles in MMNCs produce a stronger effect on the yield strength than in MMCs.

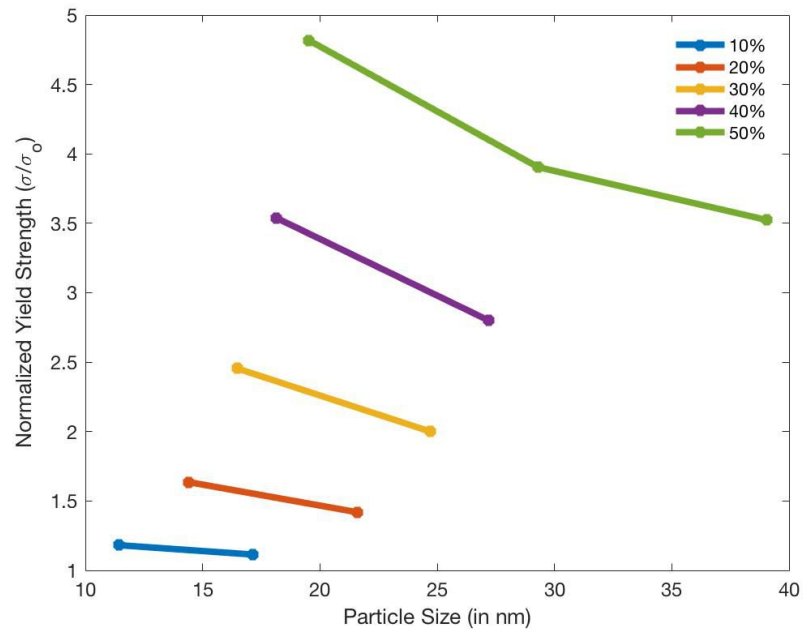


Figure 5.7: Effect of particle size and volume fraction on normalized yield strength of different specimens.

In MMCs, the inter-particle distance is of the order of few micrometers unlike in MMNCs, where it is of the order of few nanometers. To discuss more, an ob-

observation on the change in yield strength when inter-particle spacing is varied was conducted. The particle size and inter-particle distance have a linear relationship when cubic particles are used. Hence, the yield-strength vs inter-particle distance plots have a trend similar to figure 5.7.

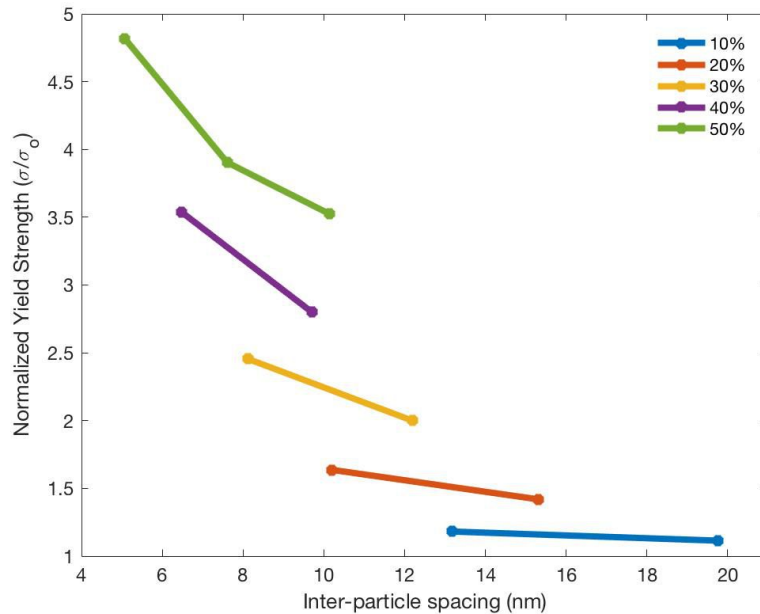


Figure 5.8: Effect of inter-particle spacing and volume fraction on normalized yield strength of different specimens.

Figure 5.8 shows the effect of inter-particle distance on the yield strength when volume fraction of the specimens is kept constant. As previously discussed in this chapter, Orowan strengthening may be the cause of this huge increase in the yield strength by decreasing the inter-particle distance. Orowan strengthening is known to occur only when the inter-particle distance is less than 100 nm, which is the case of all our simulations. The lesser the inter-particle distance, the more is this strengthening effect. Although the plots seem qualitatively convincing, precise evaluation of the strengthening of the specimens caused by Orowan effect is not done as cubic particles were used in the simulations. There was significant research on Orowan strengthening when spherical particles were used, however the

case of cubic particles was not investigated vigorously. Also, the effect of Orowan strengthening when particle volume fraction reaches as high as 50% was not researched over the last few years. So, a clear suggestion cannot be made whether Orowan strengthening is the main cause responsible for this huge increase in the yield strength.

Another probable reason for the huge increase in the yield strength of nanocomposites may be the use of cubic particles in the simulations. As cubic particles provide twice as much pinning effect as spherical particles do, the yield strength increase may also be attributed to this effect. The Orowan strengthening effect when cubic particles are used in nanocomposites has not been studied significantly.

5.4 Conclusion

Though the yield strength-volume fraction curves of the nanocomposites with ductile matrices seem qualitatively consistent with the existing continuum models, the results do not seem convincing. Unlike the continuum models, the yield strength in the case of nanocomposites vary not only with the volume fraction but also with the particle size. The results show that in the case of nanocomposites, another parameter, inter-particle spacing (which depends on the particle size in specimens with same volume fraction) also can be related to the yield strength of the nanocomposite. The effect of inter-particle spacing on the yield strength of nanocomposites was studied over the past, and the effect is known as Orowan strengthening effect.

The maximum yield strength of nanocomposites with 50% particle volume fraction is about 5 times the yield strength of Ag polycrystal with no particles. This is significantly high and cannot be just explained by the existing continuum models on high volume fraction of particles in ductile matrix. This extensive strengthening

can be partially convincing with the studies on strengthening mechanisms in the field of nanocomposites.

Experimental studies in the field of nanomaterials were done significantly over the past few decades. Various factors that depend on the strengthening of nanocomposites were documented well before. The strengthening of nanocomposites is commonly achieved by: a) Orowan strengthening b) load bearing effect c) Enhanced dislocation density mechanism.

To summarize, the results of Scanlon et al. [54] and the continuum models explored by Bao et al. [6] were taken as reference while performing the study on MMNCs in this chapter. The results in this study showed an increased effect of volume fraction on the yield strength of the nanocomposites than the results from the literature. The higher yield strength as discussed in the previous section may be attributed because of the following aspects:

1. The grains of the polycrystals chosen in this study were truncated octahedrons which are perfectly coherent to the grain structure. This case is different from the Scanlon et al.'s methodology where metal granules of irregular shapes were injected in to the ceramic targets using sputtering and the level of coherency of the metal granules with the ceramic target is unknown.
2. Cubic particles were used to investigate the particle-reinforced MMNCs in this study, which offer a very strong pinning effect in the polycrystals when compared to spherical particles.
3. The particles in the polycrystal specimens were considered as rigid and hence, their effect on the yield strength of the matrix material would be higher than that produced by ceramic particles.
4. Unlike the nature of particles in continuum models, the nano-sized particles have strong cohesion with matrix material and provide bonding at atomic

level which gives rise to an increase in the yield strength due to load bearing effect.

5. When the inter-particle spacing is less than 100 nm which is the case of the study in this chapter, Orowan strengthening is known to cause an increase in the yield strength. This mechanism is not evident in MMCs as the inter-particle spacing in micro-sized MMCs is of the order of few micrometers and hence, the increase in yield strength due to this mechanism would be negligible.

CHAPTER 6 SUMMARY AND FUTURE PROSPECTS

Nanocrystalline materials can play a vital role in applications where high yield strength materials are desired because of their outstanding mechanical properties. NC materials have higher strength because of their lower grain sizes. These NC materials can further be strengthened by adding second-phase particles. Addition of second-phase particles hinders the grain boundary motion by a mechanism called Zener pinning. The effect of Zener pinning depends on several factors such as: a) type of grain boundary b) particle size c) particle-boundary interface d) temperature e) orientation of grain boundary with the particle.

Zener pinning is significant even when the size of the second phase particles is around 0.5 nm and with a mere 0.2% volume fraction of particles in the specimens. The hindering of grain boundary motion helps in preventing grain growth in NC materials and hence, maintain the strength of the NC material. The study of Zener pinning can be extended by implementing spherical particles to assess more realistic experimental situations. The effect of high particle volume fractions in NC materials was studied in Chapter 5. The effect of volume fraction and particle size on the yield strength of the nanomaterials is studied. The nanocomposites showed that as particle size is reduced when the volume fraction of the particle phase is kept constant, an increase in the yield strength was observed. The highest increase in yield strength of nanocomposite specimens observed in this study was about 5 times time yield strength of NC specimen without any particles. This huge increase is possible only in nano-sized specimens and cannot be observed in micro-sized MMCs. Hence, nanocomposites can be used to produce ultrahigh strength structures. However, the matrix material should be ductile enough to reduce the presence of high stress concentrations that would be generated near the interface between matrix and particle phases.

In future, the research on these high particle volume fraction nanocomposites can produce some interesting insights in developing materials for applications such as in aircraft, heat-sinks, bullet-proof materials where ultrahigh strength is desired. As a part of future work, atomistic simulations on nanocomposites with a non-rigid second phase which may reveal exactly how NC materials behave with high volume fractions of particles in the specimens. Also, the study of Orowan strengthening when high volume fraction of particles is used can deduce some interesting phenomenon on how the yield strength varies with volume fraction and inter-particle spacing and also to know if Orowan strengthening is the main cause of the high yield strength observed in Chapter 5.

APPENDIX A CALCULATION OF PARTICLE SIZE AND INTER-PARTICLE SPACING IN CUBIC NC SPECIMENS

In chapter 5, cubic particles were used as reinforcements in Ag polycrystals. The volume fraction of different specimens was used to calculate the particle size, d and inter-particle spacing, r . The length of the specimens of types A, B and C used in the simulations were 24.6 nm, 36.9 nm, and 49.2 nm as mentioned in section 5.2. If the specimen length is assumed as 'a', the expression for the volume of particle can be described as

Volume of particle = (Volume fraction of particle) \times (Volume of specimen)

$$d^3 = fa^3, \quad (1)$$

where, f is the volume fraction of particle. The above equation can be simplified as

$$d = f^{1/3}a. \quad (2)$$

The inter-particle spacing, r is given by

$$r = a - d = a(1 - f^{1/3}). \quad (3)$$

The particle size and inter-particle spacing specified in tables 5.2, 5.3, and 5.4 for different specimens were calculated using the equations (2) and (3) respectively.

REFERENCES

- [1] L Lu, R Schwaiger, ZW Shan, M Dao, K Lu, and S Suresh. Nano-sized twins induce high rate sensitivity of flow stress in pure copper. *Acta materialia*, 53(7):2169–2179, 2005.
- [2] Carl C Koch, Ronald O Scattergood, Khaled M Youssef, Ethan Chan, and Yuntian T Zhu. Nanostructured materials by mechanical alloying: new results on property enhancement. *Journal of materials science*, 45(17):4725–4732, 2010.
- [3] Paul G Sanders, JA Eastman, and JR Weertman. Elastic and tensile behavior of nanocrystalline copper and palladium. *Acta materialia*, 45(10):4019–4025, 1997.
- [4] M Palombo, A Gabrielli, VDP Servedio, G Ruocco, and S Capuani. Structural disorder and anomalous diffusion in random packing of spheres. *Scientific reports*, 3:2631, 2013.
- [5] SP Ringer, Wen-Bin Li, and KE Easterling. On the interaction and pinning of grain boundaries by cubic shaped precipitate particles. *Acta Metallurgica*, 37(3):831–841, 1989.
- [6] G Bao, JW Hutchinson, and RM McMeeking. Particle reinforcement of ductile matrices against plastic flow and creep. *Acta metallurgica et materialia*, 39(8):1871–1882, 1991.
- [7] EO Hall. The deformation and ageing of mild steel: lii discussion of results. *Proceedings of the Physical Society. Section B*, 64(9):747, 1951.
- [8] NJ Petch. The cleavage strength of polycrystals. *Journal of the Iron and Steel Institute*, 174:25–28, 1953.

- [9] Cyril Stanley Smith. Grains, phases, and interfaces: An introduction of microstructure. *Trans. Metall. Soc. AIME*, 175:15–51, 1948.
- [10] L Farrissey, S Schmauder, M Dong, E Soppa, MH Poech, and P McHugh. Investigation of the strengthening of particulate reinforced composites using different analytical and finite element models. *Computational materials science*, 15(1):1–10, 1999.
- [11] DC Drucker. Engineering and continuum aspects of high-strength materials (technical report no. 7). Technical report, Brown Univ., Providence, 1964.
- [12] Deborah Elcock. Potential impacts of nanotechnology on energy transmission applications and needs. Technical report, Argonne National Lab.(ANL), Argonne, IL (United States), 2007.
- [13] Hongli Zhu, Wei Luo, Peter N Ciesielski, Zhiqiang Fang, JY Zhu, Gunnar Henriksson, Michael E Himmel, and Liangbing Hu. Wood-derived materials for green electronics, biological devices, and energy applications. *Chemical reviews*, 116(16):9305–9374, 2016.
- [14] Sarita Kango, Susheel Kalia, Annamaria Celli, James Njuguna, Youssef Habibi, and Rajesh Kumar. Surface modification of inorganic nanoparticles for development of organic–inorganic nanocomposites—a review. *Progress in Polymer Science*, 38(8):1232–1261, 2013.
- [15] Ramazan Asmatulu, P Nguyen, and Eylem Asmatulu. Nanotechnology safety in the automotive industry. In *Nanotechnology Safety*, pages 57–72. Elsevier, 2013.
- [16] Jun Chen and Fangyi Cheng. Combination of lightweight elements and nanostructured materials for batteries. *Accounts of chemical research*, 42(6):713–723, 2009.

- [17] Kazuhisa Miyoshi. Solid lubricants and coatings for extreme environments: state-of-the-art survey. 2007.
- [18] Mihail C Roco. Nanotechnology: convergence with modern biology and medicine. *Current opinion in biotechnology*, 14(3):337–346, 2003.
- [19] H. Gleiter. Nanocrystalline materials. *Progress in Materials Science*, 33(4):223 – 315, 1989.
- [20] Mea Legros, BR Elliott, MN Rittner, JR Weertman, and KJ Hemker. Microsample tensile testing of nanocrystalline metals. *Philosophical magazine A*, 80(4):1017–1026, 2000.
- [21] Neil Farbstein. Ultra high strength nanomaterials and methods of manufacture, August 28 2018. US Patent App. 14/488,452.
- [22] RW Armstrong. The (cleavage) strength of pre-cracked polycrystals. *Engineering Fracture Mechanics*, 28(5-6):529–538, 1987.
- [23] N Ono, R Nowak, and S Miura. Effect of deformation temperature on hall–petch relationship registered for polycrystalline magnesium. *Materials Letters*, 58(1-2):39–43, 2004.
- [24] Jakob Schiøtz and Karsten W Jacobsen. A maximum in the strength of nanocrystalline copper. *Science*, 301(5638):1357–1359, 2003.
- [25] Brian Lawn and T Rodney Wilshaw. *Fracture of brittle solids*. Cambridge university press, 1993.
- [26] William D Callister. *Materials science and engineering-an introduction*. John wiley & sons, 2007.
- [27] Helena Van Swygenhoven and Julia R Weertman. Deformation in nanocrystalline metals. *Materials today*, 9(5):24–31, 2006.

- [28] AH Chokshi, A Rosen, J Karch, and H Gleiter. On the validity of the hall-petch relationship in nanocrystalline materials. *Scripta Metallurgica*, 23(10):1679–1683, 1989.
- [29] El Arzt. Size effects in materials due to microstructural and dimensional constraints: a comparative review. *Acta materialia*, 46(16):5611–5626, 1998.
- [30] Jakob Schiøtz, Francesco D Di Tolla, and Karsten W Jacobsen. Softening of nanocrystalline metals at very small grain sizes. *Nature*, 391(6667):561, 1998.
- [31] CE Carlton and PJ Ferreira. What is behind the inverse hall–petch effect in nanocrystalline materials? *Acta Materialia*, 55(11):3749–3756, 2007.
- [32] Marc A Meyers, A Mishra, and David J Benson. Mechanical properties of nanocrystalline materials. *Progress in materials science*, 51(4):427–556, 2006.
- [33] HJ Höfler and RS Averback. Grain growth in nanocrystalline TiO₂ and its relation to vickers hardness and fracture toughness. *Scripta Metallurgica;(United States)*, 24(12), 1990.
- [34] Sidney Yip. Nanocrystals: the strongest size. *Nature*, 391(6667):532, 1998.
- [35] Adrian P Sutton. Interfaces in crystalline materials. *Monographs on the Physice and Chemistry of Materials*, pages 414–423, 1995.
- [36] Gunter Gottstein and Lasar S Shvindlerman. *Grain boundary migration in metals: thermodynamics, kinetics, applications*. CRC press, 2009.
- [37] Farah Hammami and Yashashree Kulkarni. Rate dependence of grain boundary sliding via time-scaling atomistic simulations. *Journal of Applied Physics*, 121(8):085303, 2017.

- [38] John W Cahn, Yuri Mishin, and Akira Suzuki. Coupling grain boundary motion to shear deformation. *Acta materialia*, 54(19):4953–4975, 2006.
- [39] Yixiong Liu and BR Patterson. Stereological analysis of zener pinning. *Acta materialia*, 44(11):4327–4335, 1996.
- [40] Bimal K Kad and Peter M Hazzledine. Monte carlo simulations of grain growth and zener pinning. *Materials Science and Engineering: A*, 238(1):70–77, 1997.
- [41] RK Koju, KA Darling, LJ Kecskes, and Y Mishin. Zener pinning of grain boundaries and structural stability of immiscible alloys. *JOM*, 68(6):1596–1604, 2016.
- [42] Manohar PA, M Ferry, and T Chandra. Five decades of the zener equation. *ISIJ international*, 38(9):913–924, 1998.
- [43] Dengke Chen, Tarek Ghoneim, and Yashashree Kulkarni. Effect of pinning particles on grain boundary motion from interface random walk. *Applied Physics Letters*, 111(16):161606, 2017.
- [44] T Christman, A Needleman, and S Suresh. An experimental and numerical study of deformation in metal-ceramic composites. *Acta Metallurgica*, 37(11):3029–3050, 1989.
- [45] G Bao and F Zok. On the strength of ductile particle reinforced brittle matrix composites. *Acta metallurgica et materialia*, 41(12):3515–3524, 1993.
- [46] E Pagounis and VK Lindroos. Processing and properties of particulate reinforced steel matrix composites. *Materials Science and Engineering: A*, 246(1-2):221–234, 1998.

- [47] NA Travitzky. Effect of metal volume fraction on the mechanical properties of alumina/aluminum composites. *Journal of materials science*, 36(18):4459–4463, 2001.
- [48] Shao-Yun Fu, Xi-Qiao Feng, Bernd Lauke, and Yiu-Wing Mai. Effects of particle size, particle/matrix interface adhesion and particle loading on mechanical properties of particulate–polymer composites. *Composites Part B: Engineering*, 39(6):933–961, 2008.
- [49] J Sleziona, J Wieczorek, and M Dyzia. Mechanical properties of silver matrix composites reinforced with ceramic particles. *Journal of Achievements in Materials and Manufacturing Engineering*, 17(1-2), 2006.
- [50] FA Mirza and DL Chen. A unified model for the prediction of yield strength in particulate-reinforced metal matrix nanocomposites. *Materials*, 8(8):5138–5153, 2015.
- [51] HX Peng, Z Fan, and JRG Evans. Bi-continuous metal matrix composites. *Materials Science and Engineering: A*, 303(1-2):37–45, 2001.
- [52] SF Hassan and M Gupta. Development of high performance magnesium nanocomposites using solidification processing route. *Materials Science and Technology*, 20(11):1383–1388, 2004.
- [53] Zhe Zhang and DL Chen. Consideration of orowan strengthening effect in particulate-reinforced metal matrix nanocomposites: A model for predicting their yield strength. *Scripta Materialia*, 54(7):1321–1326, 2006.
- [54] MR Scanlon and RC Cammarata. Mechanical properties of nanocomposite granular metal thin films. *Journal of applied physics*, 76(6):3387–3393, 1994.
- [55] D Tabor. The hardness and strength of metals. *J. Inst. Metals*, 79:1, 1951.

- [56] Ian M Hutchings. The contributions of david tabor to the science of indentation hardness. *Journal of Materials Research*, 24(3):581–589, 2009.
- [57] Michael P Allen. Introduction to molecular dynamics simulation. *Computational soft matter: from synthetic polymers to proteins*, 23:1–28, 2004.
- [58] Steve Plimpton. Fast parallel algorithms for short-range molecular dynamics. *Journal of computational physics*, 117(1):1–19, 1995.
- [59] John Edward Jones. On the determination of molecular fields-II. from the equation of state of a gas. *Proc. R. Soc. Lond. A*, 106(738):463–477, 1924.
- [60] Murray S Daw and Michael I Baskes. Embedded-atom method: Derivation and application to impurities, surfaces, and other defects in metals. *Physical Review B*, 29(12):6443, 1984.
- [61] Murray S Daw, Stephen M Foiles, and Michael I Baskes. The embedded-atom method: a review of theory and applications. *Materials Science Reports*, 9(7-8):251–310, 1993.
- [62] RA Johnson. Analytic nearest-neighbor model for fcc metals. *Physical Review B*, 37(8):3924, 1988.
- [63] Magnus Rudolph Hestenes and Eduard Stiefel. *Methods of conjugate gradients for solving linear systems*, volume 49. NBS Washington, DC, 1952.
- [64] Alexander Stukowski. Visualization and analysis of atomistic simulation data with ovito—the open visualization tool. *Modelling and Simulation in Materials Science and Engineering*, 18(1):015012, 2009.
- [65] Dennis C Rapaport and Dennis C Rapaport Rapaport. *The art of molecular dynamics simulation*. Cambridge university press, 2004.

- [66] Jarosaw Meller. Molecular dynamics. *Encyclopedia of life sciences*, pages 1–8, 2001.
- [67] Martin Karplus and Gregory A Petsko. Molecular dynamics simulations in biology. *Nature*, 347(6294):631, 1990.
- [68] MA Tschopp and DL McDowell. Asymmetric tilt grain boundary structure and energy in copper and aluminium. *Philosophical Magazine*, 87(25):3871–3892, 2007.
- [69] MA Tschopp and DL McDowell. Structures and energies of Σ 3 asymmetric tilt grain boundaries in copper and aluminium. *Philosophical Magazine*, 87(22):3147–3173, 2007.
- [70] Yu Mishin, MJ Mehl, DA Papaconstantopoulos, AF Voter, and JD Kress. Structural stability and lattice defects in copper: Ab initio, tight-binding, and embedded-atom calculations. *Physical Review B*, 63(22):224106, 2001.
- [71] Haoyue Zhang, Nikica Maljkovic, and Brian S Mitchell. Structure and interfacial properties of nanocrystalline aluminum/mullite composites. *Materials Science and Engineering: A*, 326(2):317–323, 2002.
- [72] Haozhe Liu, Aimin Wang, Luhong Wang, Bingzhe Ding, Zhuangqi Hu, and Hongying Peng. The syntheses of SiC_p/Al nanocomposites under high pressure. *Journal of materials research*, 12(5):1187–1190, 1997.
- [73] Xiao Chen and Hermann J Schluesener. Nanosilver: a nanoproduct in medical application. *Toxicology letters*, 176(1):1–12, 2008.
- [74] J Wesley Alexander. History of the medical use of silver. *Surgical infections*, 10(3):289–292, 2009.

- [75] Ram Prasad, Atanu Bhattacharyya, and Quang D Nguyen. Nanotechnology in sustainable agriculture: recent developments, challenges, and perspectives. *Frontiers in microbiology*, 8:1014, 2017.
- [76] Ping Li, Juan Li, Changzhu Wu, Qingsheng Wu, and Jian Li. Synergistic antibacterial effects of β -lactam antibiotic combined with silver nanoparticles. *Nanotechnology*, 16(9):1912, 2005.
- [77] Oleg V Salata. Applications of nanoparticles in biology and medicine. *Journal of nanobiotechnology*, 2(1):3, 2004.
- [78] Susan WP Wijnhoven, Willie JGM Peijnenburg, Carla A Herberts, Werner I Hagens, Agnes G Oomen, Evelyn HW Heugens, Boris Roszek, Julia Bisschops, Ilse Gosens, Dik Van De Meent, Susan Dekkers, Wim H De Jong, Maaike van Zijverden, Adrinne JAM Sips, and Robert E Geertsma. Nano-silver—a review of available data and knowledge gaps in human and environmental risk assessment. *Nanotoxicology*, 3(2):109–138, 2009.
- [79] Dongjo Kim and Jooho Moon. Highly conductive ink jet printed films of nanosilver particles for printable electronics. *Electrochemical and Solid-State Letters*, 8(11):J30–J33, 2005.
- [80] Matthias Knoerr, Silke Kraft, and Andreas Schletz. Reliability assessment of sintered nano-silver die attachment for power semiconductors. In *Electronics Packaging Technology Conference (EPTC), 2010 12th*, pages 56–61. IEEE, 2010.
- [81] Seung H Ko, Heng Pan, Costas P Grigoropoulos, Christine K Luscombe, Jean MJ Fréchet, and Dimos Poulikakos. All-inkjet-printed flexible electronics fabrication on a polymer substrate by low-temperature high-resolution selec-

- tive laser sintering of metal nanoparticles. *Nanotechnology*, 18(34):345202, 2007.
- [82] Georgina Miller, Darren van Schaik, and R Adelaide. *Nanotechnology in food and agriculture*. Radio Adelaide, 2008.
- [83] Sandhya Mishra and HB Singh. Biosynthesized silver nanoparticles as a nanoweapon against phytopathogens: exploring their scope and potential in agriculture. *Applied microbiology and biotechnology*, 99(3):1097–1107, 2015.
- [84] P L Williams, Y Mishin, and J C Hamilton. An embedded-atom potential for the cu ag system. *Modelling and Simulation in Materials Science and Engineering*, 14(5):817, 2006.
- [85] Ju Li. Atomeye: an efficient atomistic configuration viewer. *Modelling and Simulation in Materials Science and Engineering*, 11(2):173, 2003.
- [86] Sergei Vlassov, Boris Polyakov, Leonid M Dorogin, Mikk Antsov, Magnus Mets, Madis Umalas, Rando Saar, Rünno Lõhmus, and Ilmar Kink. Elasticity and yield strength of pentagonal silver nanowires: In situ bending tests. *Materials Chemistry and Physics*, 143(3):1026–1031, 2014.
- [87] Yong Zhu, Qingquan Qin, Feng Xu, Fengru Fan, Yong Ding, Tim Zhang, Benjamin J Wiley, and Zhong Lin Wang. Size effects on elasticity, yielding, and fracture of silver nanowires: In situ experiments. *Physical review B*, 85(4):045443, 2012.